Variability of temperature and ozone in the upper troposphere and lower stratosphere from multi-satellite observations and reanalysis data

Ming Shangguan[1], Wuke Wang[2,3,4], and Shuanggen Jin[5,6]

[1]School of Transportation,Southeast University, Nanjing 21189, China
[2]Institute for Climate and Global Change Research, School of Atmospheric Sciences, Nanjing University, Nanjing 210023, China
[3]Joint International Research Laboratory of Atmospheric and Earth System Sciences (JirLATEST), Nanjing University, Nanjing 210023, China
[4]Collaborative Innovation Center of Climate Change, Jiangsu Province, Nanjing 210023, China
[5]Shanghai Astronomical Observatory,Chinese Academy of Sciences, Shanghai 200030, China
[6]School of Remote Sensing and Geomatics Engineering, Najing University of Information Science and Technology, Nanjing 210044, China

Correspondence: Ming Shangguan(sgming@seu.edu.cn), Wuke Wang(wuke.wang@nju.edu.cn)

Abstract. Temperature and ozone changes in the upper troposphere and lower stratosphere (UTLS) are important components of climate change. In this paper, variability and trends of temperature and ozone in the UTLS are investigated for the period 2002-2017 using the high quality, high vertical resolution GNSS RO data and improved merged satellite data sets. As part of the Stratosphere-troposphere Processes And their Role in Climate (SPARC) Reanalysis Intercomparison Project (S-RIP), three reanalysis data sets including the ERA-I, MERRA2 and the recently released ERA5 are evaluated for their representation of temperature and ozone in the UTLS. The recent temperature and ozone trends are updated by a multiple linear regression (MLR) method, and related to Sea Surface Temperature (SST) changes based on model simulations with NCAR's Whole Atmosphere Community Climate Model (WACCM).

All reanalysis temperatures show good agreement with the GNSS RO measurements in both absolute values and annual cycle. Interannual variations of temperature related to QBO and ENSO processes are well represented by all reanalyses. However, evident biases can be seen in reanalyses for the linear trends of temperature since they are affected by discontinuities in assimilated observations and methods. Such biases can be corrected and the estimated trends can be significantly improved. ERA5 is significantly improved compared with ERA-I and shows the best agreement with the GNSS RO temperature.

The MLR results indicate a significant warming of 0.2-0.3 $\mathrm{K/decade}$ in most areas of the troposphere with stronger increase of 0.4-0.5 $\mathrm{K/decade}$ in mid-latitudes of both hemispheres. In contrast, the stratospheric temperature decreases at a rate of 0.1-0.3 $\mathrm{K/decade}$, which is most significant in the Southern Hemisphere (SH). Positive temperature trends of 0.1-0.3 $\mathrm{K/decade}$ are seen in the tropical lower stratosphere (100-50 hPa). Negative trends of ozone are found in Northern hemisphere (NH) at 150-50 hPa while positive trends are evident in the tropical lower stratosphere. Asymmetric trends of ozone can be found in the mid-latitudes of two hemispheres in the middle stratosphere, with significant ozone decrease in NH and increase of ozone in the SH. Large biases exist in reanalyses and it is still challenging to do trend analysis based on reanalysis ozone data.

According to single-factor-controlling model simulations with WACCM, the temperature increase in the troposphere as well as ozone decrease in the NH stratosphere are mainly connected to the increase of SST and subsequent changes of atmospheric circulations. Both the increase of SSTs and the decrease of ozone in the NH contribute to the temperature decrease in the NH stratosphere. The increase of temperature in the lower stratospheric tropics may be related to an increase of ozone in that region, while SST increase contributes to a cooling in that area.

1 Introduction

The upper troposphere and lower stratosphere (UTLS) is a key region for stratosphere-troposphere coupling and affects the content of trace gases in both the troposphere and the stratosphere (Staten and Reichler, 2008; Fueglistaler et al., 2014). Temperature change in the UTLS is an important component of climate change and has been greatly concerned by numerous studies (Randel et al., 2009; Wang et al., 2012; Kim et al., 2013; Wang et al., 2013). While measurements in the UTLS are relatively sparse, reanalysis data are widely used to investigate temperature variabilities (Xie et al., 2012; Wang et al., 2016). Atmospheric reanalysis data assimilate ground-based, satellite-based, and other data sources to provide the current best estimation of the real atmosphere with global spatial and temporal coverage. However, because of the lacking of high quality and high vertical resolution temperature observations and also the low vertical resolution of the model, the reanalysis data in the UTLS might be problematic (Zhao and Li, 2006; Trenberth and Smith, 2006, 2009). How accuracy the temperature field as well as its variability are represented in reanalysis data is required to be quantified.

A comprehensive assessment of the accuracy of the reanalysis temperature has been challenging because of the lacking of high quality observations with high temporal and high spacial resolution. For example, ground-based radiosonde measurements often have low temporal and spatial resolution (distributed in the northern hemisphere mostly), while nadir sounding satellite measurements (e.g., Microwave Sounding Unit) can not well resolve the narrow vertical-scale features in the UTLS. Global Navigation Satellite System Radio Occultation (GNSS RO) is a relatively new technology which measures the time delay in occulted signals from one satellite to another and provides information to derive profiles of atmospheric temperature and moisture. Since the Challenging Minisatellite Payload (CHAMP) mission launched in 2001, GNSS RO has provided high quality and high vertical resolution temperature measurements in the UTLS for almost two decades. Due to its self-calibrating and not susceptible to instrument drift (Anthes et al., 2008), the GNSS RO provides a stable temperature record which is well suited to validate the reanalysis data.

Atmospheric reanalysis has been developed for decades. While more and more observations are available and more advanced techniques are used in the assimilation system, new generation of reanalysis is expected to be significantly improved. The European Center for Medium-Range Weather Forecasts (ECMWF) released its fifth generation reanalysis (ERA5) in 2017. It is very interesting to see how the quality of temperatures in the UTLS has been improved in ERA5. The primary goal of this study is to evaluate the UTLS temperature in the newest ERA5 reanalysis using the GNSS RO as a reference. Within the context of the SPARC S-RIP, the Modern-Era Retrospective analysis for Research and Application, Version 2 (MERRA2) and the ERA-Interim (ERA-I) are also included for a comparison.

To give a comprehensive assessment of the reanalysis temperature in the UTLS, the interannual variations as well as the long-term trend of temperature are compared between the GNSS RO and different reanalysis data sets. Interannual variabilities of temperatures in the UTLS are related to complex processes, such as the Quasi-Biennial Oscillation (QBO) and the El-Niño Southern Oscillation (ENSO) (Xie et al., 2012; Randel and Wu, 2015; Garfinkel et al., 2018). QBO and ENSO related temperature signals in the UTLS are analyzed to evaluate the capability of reanalysis data to well represent QBO and ENSO related signals. While assimilating many types of observations, reanalysis data suffer from instrument exchanges and may exhibit sudden changes as new data are assimilated (Sturaro, 2003; Sterl, 2004). Such discontinuities may strongly influence the long-term trend calculated from reanalysis data. How well could the reanalysis data represent the interannual variability as well as long-term trend of temperatures in the UTLS is the second goal of this study.

Long-term trend is a key issue regarding to the UTLS researches. A net cooling in the stratosphere was seen over the past decades (Randel et al., 2009; Flato et al., 2014). However, large discrepancies of the temperature trends in the UTLS have been reported between different observational/reanalysis data sets (Wang et al., 2012; Xie et al., 2012) and also between data and models (Kim et al., 2013). Recently, a slowing down of cooling in the lower stratosphere since 1998 (Polvani et al., 2017), or an increase of temperature in the tropical tropopause layer since 2001 (Wang et al., 2013) has been reported, which makes it more complicated to fully understand the UTLS temperature trend. Temperature changes in the UTLS are related to both internal processes, e.g. SST variations, and external forcing, such as greenhouse gases (GHG) and ozone-depleting substances (ODS) (Randel et al., 2009; Flato et al., 2014). If the slowing down or changing in sign of temperature in the UTLS persists in future is an open question. Whether the turning of temperature trends around 2000 is related to internal processes like SST variations (Wang et al., 2015, 2016), or caused by ozone changes (Polvani and Solomon, 2012; Polvani et al., 2017) is still not clear. The third goal of this study is to update the recent temperature trend in the UTLS using a combination of GNSS RO and reanalysis data sets and attribute it to different factors like SST and ozone changes.

To understand the relationship between ozone and temperature changes in the UTLS, the recent variability of ozone is also analyzed. Ozone is closely coupled to temperature changes in the UTLS. Abalos et al. (2012) studied the temporal variability of the upwelling near the tropopause using MLS (Microwave Limb Sounder) ozone/CO and ERA-I temperature/wind and demonstrated the high correlations between the upwelling, temperatures and tracers. Schoeberl et al. (2008) found that photochemical processes force fluctuations in the trace gases (such as ozone) to be synchronized with annual and QBO variations in the zonal mean residual vertical velocity. Changes in ozone concentrations may impact temperature directly through its radiative effects (Forster et al., 2007; Abalos et al., 2012; Maycock, 2016; Gilford et al., 2016) or indirectly through its modulation to atmospheric circulations (Polvani et al., 2017). The recent variability of ozone in the UTLS has been investigated by several studies. Harris et al. (2015) found some negative trend in the tropics and positive trends in the lower stratosphere at mid-latitudes based on the merged satellite ozone data from 1998 to 2012. Steinbrecht et al. (2017) updated the ozone trends for the period 2000 to 2016 and found a decreasing ozone in the tropics and at northern mid-latitude between 100 and 50 hPa. Ball et al. (2018) also indicated a continuous decline in the lower stratosphere (147-30 hPa at mid-latitudes or 100-32 hPa at tropical latitudes) from multiple satellite ozone data between 1998 and 2016. Chipperfield et al. (2018) extended the analysis to 2017 and argued that

the ozone decline in the lower stratosphere is insignificant. Whether the ozone is increasing or declining recently is still under debate, while its relationship to temperature trends awaits further investigations.

This study revisits the recent variability of ozone in the UTLS by a combination of the SWOOSH (Stratospheric Water and OzOne Satellite Homogenized) and the C3S (Copernicus Climate Change Service) merged satellite ozone data sets. At the same time, ozone content is provided in almost all current reanalysis due to its important impact on stratospheric temperature (Dee et al., 2011; Davis et al., 2017; Wargan et al., 2017). A comprehensive assessment of ozone data in reanalysis has been made by a previous study (Davis et al., 2017). However, the newest ERA5 reanalysis was not included in their study. As part of the SPARC S-Rip, ozone records from different reanalyses (ERA5 and MERRA2) are also analyzed and compared to merged satellite data sets in this study.

Coupled chemistry climate models are useful tools and have been widely used to attribute climate variability. A series of model simulations with NCAR's WACCM are used in this study to fully understand the exact reason of the recent temperature variability in the UTLS. WACCM is one of the two available atmospheric components of the Community Earth System Model (CESM), and has been used widely in previous studies to detect and attribute the variabilities of temperature and ozone in the UTLS (Wang et al., 2015; Randel et al., 2017). In this study, single factor controlling simulations are conducted to quantify the relative contribution of different climate forcing.

The paper is laid out as follows: In sect. 2 we provide an overview of the used observational data sets, reanalyses, model and method for trend calculation. In sect. 3 we compare and analyze the temperature and ozone in absolute mean, anomalies and trend in vertically, regionally and globally. In the final section, we conclude with a summary.

2 Data and Methods

2.1 GNSS RO Temperature Data

The Challenging Minisatellite Payload (CHAMP) became operational and produce 150 occultation events globally per day in 2001 (Wickert et al., 2001). Nearly one decade CHAMP data are available from May 2001 to Oct. 2008. In 2006 the Constellation Observing System for Meteorology, Ionosphere and Climate (COSMIC), which is a constellation of six satellites, providing more than 10 times the number of observations (1000-3000 occultations per day). According to previous studies (Foelsche et al., 2008; Ho et al., 2009) , the mean temperature differences between the collocated soundings COSMIC and CHAMP were within 0.1 K from 200 to 20 hPa. Many studies have demonstrated that GNSS RO temperature data have good quality in the range of 8-30 km (Schmidt et al., 2005, 2010; Ho et al., 2012). Ho et al. (2009) found that results from GNSS RO show a mean temperature deviation of 0.05 K with a standard deviation of 1 K in the range of 8-30 km. GNSS RO data are high precision and can be used to assess the accuracy of other detection techniques such as to correct the temperature bias of radiosondes in the lower stratosphere (Ho et al., 2016). Many reanalyses have already assimilated GNSS RO bending angles.

In our study, we make use of monthly mean temperature data at 400-10 hPa (approximately 6.5-30 km) for the trend analysis, with which the essential atmospheric variability has already been captured by a single satellite (Pirscher et al., 2007; Foelsche et al., 2008; Ladstädter et al., 2011). Note that the region of 400-10 hPa is out of the definition of UTLS, which

is usually defined as the region ±5 km of the tropopause. Here we focus on a broader region from the upper troposphere (400 hPa) to the mid stratosphere (10 hPa) due to the availability of GNSS RO temperature. More than 100 observations per month per 5 latitude grid can be provided by single satellite CHAMP. Much improved spatial coverage (more than 10 times number of profiles) appear since late 2006 due to the start of COSMIC mission. The high latitudes regions with low coverage of observations can cause large sampling errors. In consideration of large uncertainties caused by sparse data coverage at high latitudes, we consider only GNSS RO data in latitude bands 60°S to 60°N here. According to previous studies (Foelsche et al., 2008; Scherllin-Pirscher et al., 2011; Ladstädter et al., 2011) the sampling errors have low effect (<0.2 K) on the trend calculation in mid-latitudes and tropics. The moisture-corrected atmospheric temperature profile (wetPrf) products of CHAMP and COSMIC provided by the UCAR COSMIC Data Analysis and Archive Center (CDAAC) are utilized. WetPrf products using one-dimensional variational method (1DVAR) have up to 100 m vertical resolution from 0.1 to 40 km and use low resolution ECMWF ERA-I profiles as background for 1DVAR technique (Wee and Kuo, 2015). The RO data we use in this study are processed in reprocessed and post-processed categories, which can provide stable and accurate observations for climate studies. The CHAMP wetPf2 version is 2016.2430 and COSMIC wetPrf version is 2013.3520 and 2016.1120.

Monthly zonal means on standard pressure levels (400, 350, 300, 250, 225, 200, 175, 150, 125, 100, 70, 50, 30, 20, 10 hPa) were determined, whereas 5°N non-overlapping latitude bands centered at 57.5°S-57.5°N were used. Larger discrepancies were observed for pressure levels above 400 hPa (below 6.5 km altitudes) due to high level of moisture in the lower troposphere (Kuo et al., 2004; Kuleshov et al., 2016). Therefore we focus on the data from 400 to 10 hPa in this work. The determination of monthly zonal means were performed in four steps. Firstly, all data in a given latitude bin were averaged and standard deviation of GNSS RO with 100 m interval height are calculated. Secondly, all data were re-read and data exceeding 3 times of the standard deviation from the first zonal mean were removed as outliers at 400 levels. Thirdly, GNSS RO temperature profiles were interpolated to the standard pressure levels using piecewise linear interpolation with logarithm pressure and if there existed large gaps in the profiles, no interpolation is made. In the last step the interpolated profiles are averaged to monthly mean temperatures on 17 standard pressure levels and 24 latitude bins. Monthly means with data points less than 20 observations per latitude bin are excluded for the trend analysis. Because the earliest available CHAMP data is since May 2001, we chose a 16 years time period from 2002 to 2017 for the temperature trend calculations.

2.2 Merged satellite Ozone Data

SWOOSH data set is a merged monthly mean of stratospheric ozone measurements taken by a number of limb sounding and solar occultation satellites from 1984 to present, and includes data from the SAGE-II (v7)/III(v4), UARS HALOE (v19), UARS MLS (v5/6), and Aura MLS (v4.2) instruments (Davis et al., 2016). The measurements are homogenized by applying corrections that are calculated from data taken during time periods of instrument overlap. The merged product without interpolation based on a weighted mean of the available measurements is used in this study on the pressure levels (316, 261, 215, 178, 147, 121, 100, 83, 68, 56, 46, 38, 32, 26, 22, 18, 15, 12, 10 hPa). SWOOSH uses SAGE-II as the reference for ozone data, to which other ozone measurements are adjusted. After Aug. 2004 the SWOOSH merged product is essentially the v4.2 Aura MLS data. The SWOOSH data used in this work is version 2.6 in 5° latitude zones monthly means.

For better study the ozone variability, an independent data sets namely C3S SAGE-II/CCI/OMPS ozone products version 3 with 10° latitude bands are used. Compared with SWOOSH, The data merged 7 satellite instruments, including three instruments on board Envisate, Michelson Interferometer for Passive Atmospheric Sounding (MIPAS 2002-2012), Global Ozone Monitoring by Occultation of Stars (GOMOS 2002-2011), SCanning Imaging Spectrometer for Atmospheric CHartographY (SCIAMACHY 2002-2012), as well as Optical Spectrograph and InfraRed Imaging System (OSIRIS 2001-), SAGE-II(1984-2005), Ozone Mapping and Profiler Suite (OMPS 2012-) and Atmospheric Chemistry Experiment Fourier Transform Spectrometer (ACE-FTS 2004-) (Sofieva et al., 2017). The absolute ozone values are adjusted to the mean of SAGE-II and OSIRIS ozone profiles in 2002-2005 (which nearly coincide also with GOMOS data). Ozone profile data are provided on an altitude grid and ancillary information is provided with the data products to allow conversion unit. The data records combine a large number of high quality limb and occultation sensors. The evaluation of ozone trends using the merged C3S data with other data sets has been done by previous studies (Sofieva et al., 2017; Steinbrecht et al., 2017). The results show a good agreement between C3S and other data sets and the best quality of the merged data set is in the stratosphere in the latitude zone from 60° S to 60°N. The altitude levels (from 10 to 50 km in steps of 1 km) are interpolated to pressure levels using linear interpolation in log-presssure space. The monthly mean ozone molar concentration are converted to volume mixing ratio using the mean temperature provided by the C3S data.

2.3 Reanalysis Data

ERA-I covers the period from 1979 until present, assimilating observational data from various satellites, buoys, radiosondes, commercial aircraft and others (Dee et al., 2011). ERA-I includes GNSS RO bending angels from CHAMP, COSMIC, GRACE, MetOp, and TerraSAR-X and satellite vertical ozone profiles from GOME/GOME-2, MIPAS, MLS, SBUV (Dee et al., 2011; Davis et al., 2017). Description of the ozone system and assessments of its quality have been provided by Dee et al. (2011); Dragani (2011). In this work, monthly means of ERA-I data (2.5°x2.5°) were averaged onto 5° latitude bins. ERA-I reanalysis is widely used for inter-comparisons and currently used as background information for wetPrf. For these reasons, we choose it for the comparison.

The newest ERA5 reanalysis, which is released by ECMWF in 2018, is also used. Compared to ERA-I, ERA5 data assimilation system uses the new version of the integrated Forecasting System (IFS Cycle 41r2) instead of IFS Cycle 31r2 by ERA-I. In addition, various newly reprocessed data sets, recent instruments and cell-pressure correction SSU, improved bias correction for radiosondes etc, are renewed in ERA5. More information can be found in ERA5 data documentation https://confluence.ecmwf.int/display/CKB/ERA5+data+documentation#ERA5datadocumentation-Observations. Ozone and temperature monthly means at 17 standard pressure levels from 400 to 10 hPa are selected in this study.

MERRA2 is the latest atmospheric reanalysis of NASA's Global Modeling and Assimilation Office (GMAO) with data resolution 0.5°x0.625° (Gelaro et al., 2017). For analysis we use monthly mean assimilated ozone and temperature data on pressure levels (Modeling and Office, 2015). In conformity with ERA-I, the MERRA2 data were averaged onto 5° latitude bins with weighted mean method. Compared with ERA-I/ERA5, MERRA2 starts to assimilate GNSS RO beginning in Jul. 2004 and MLS ozone data beginning in Oct. 2004 (earlier SBUV observations) (McCarty et al., 2016). For ozone data MERRA2

assimilated MLS instead of SBUV since Oct. 2004 (Gelaro et al., 2017). Monthly means of data at 15 standard pressure levels (400, 350, 300, 250, 200, 150, 100, 70, 50, 40, 30, 20, 10 hPa) are selected for the study. Wargan et al. (2017) provided a comprehensive description and validation of the MERRA2 ozone product.

2.4 Model simulations

The Whole Atmosphere Community Climate Model, version 4 (WACCM4) is used here in its atmosphere-only mode. The horizontal resolution of the WACCM4 runs presented here is $1.9^\circ \times 2.5^\circ$ (latitude $\times$ longitude). More details of this model are described in Marsh et al. (2013). WACCM4 uses the finite-volume dynamical core with 66 standard vertical levels (about 1 km vertical resolution in the UTLS). Here we use the special version with finer vertical resolution, WACCM_L103 (Gettelman and Birner, 2007), with 103 vertical levels and about 300 m vertical resolution in the UTLS. This high vertical resolution version has been proved to better represent the detailed thermal structure as well as interannual-to-decadal variations in the UTLS (Wang et al., 2013, 2015).

A hindcast simulation (hereafter termed as the Transient run) was done for the period 1995-2017 to reproduce the recent temperature and ozone variability in the UTLS. The model was forced by observed Greenhouse Gases (GHGs), ozone depleting substances (ODSs) and solar irradiances, nudged QBO (Quasi-Biennial Oscillation) (Matthes et al., 2010) and prescribed SSTs (using the HadISST data set (Rayner et al., 2003)). The first 7 years (1995-2001) are not analyzed for a spin-up. Based on this simulation, a FixSST run was integrated for the same period and using the same climate forcing except that SSTs were fixed to climatological values. The differences between these two simulations help to estimate the contribution of SST changes to temperature and ozone trends.

2.5 Trend Calculations

From the monthly zonal mean time series the seasonal cycle is firstly calculated, and monthly zonal anomalies are estimated by subtracting the seasonal cycle from each individual monthly mean. This data analysis is performed for each data set and zonal bin. The calculated anomalies are the basis for trend calculations. The QBO and ENSO (El-Niño Southern Oscillation) are the most important phenomena that affects interannual variability of the UTLS. To exclude the effects of QBO and ENSO, we apply a multiple linear regression (MLR) based on the temperature monthly anomalies (Eq. 1) (von Storch and Zwiers, 2002).

$$y(t) = a_0 + a_1 \cdot t + a_2 \cdot ENSO(t) + a_3 \cdot QBO50(t) + a_4 \cdot QBO30(t) \tag{1}$$

The regression coefficients comprise a constant a_0, the trend coefficient a_1, the ENSO coefficient a_2, the QBO coefficients a_3 and a_4. The QBO30 and QBO50 indexes for the period 2002-2017 are normalized to unit variance from the CDAS Reanalysis data, which are the zonally averaged winds at 30 and 50 hPa and taken from over the equator (http://www.cpc.ncep.noaa.gov/data/indices/). The ENSO MEI indexes are obtained from NOAA on the six main observed variable (sea-level pressure, zonal and meridional components of the surface wind, sea surface temperature, surface air temperature and total cloudiness fraction of the sky) over the tropical Pacific (http://www.cdc.noaa.gov/people/klaus.wolter/MEI/table.html). A two month time lag for

the ENSO index is used following previous studies (Randel and Wu, 2015; Randel et al., 2017). The two-sided Student's t test is used to test for a significant linear regression relationship between the response variable and the predictor variables. The significance level is set to be 95%.

3 Results and Analysis

3.1 Time series of temperature

Figure 1 shows the initial time series of zonal mean temperature at 250 hPa from the GNSS RO observations and different reanalyses (ERA5, MERRA2 and ERA-I) as well as their differences between reanalyses and the GNSS RO data. Three latitude bands are selected to indicate temperature variations in the tropics (TP, 10°S-10°N), mid-latitudes in the NH (NM, 25°N-45°N) and mid-latitudes in the SH (SM, 25°S-45°S). Seasonal variations are relatively small in the tropics while evident annual cycle can be seen in mid-latitudes of both hemispheres. Generally, reanalyses show good agreement with the GNSS RO in monthly absolute values as well as seasonal variations except that MERRA2 shows obviously positive bias compared with other data sets in the TP. Seen from the differences between reanalyses and the GNSS RO, the bias of ERA5 and ERA-I are less than 0.5 K except in mid-latitude for the period 2002-2006, which shows bias up to 1 K. As the 5th generation of the ECMWF reanalysis, ERA5 shows slightly better agreement than ERA-I in the tropics. Temperature in ERA-I is obviously warmer than the GNSS RO of about 0.1-0.2 K, while ERA5 temperature shows differences of less than 0.1 K compared with the GNSS RO data. Warm biases (0.2 K in NM/SM and 0.7 K in TP) are seen for MERRA2 in all selected regions, which is over 1 K for the period 2002-2006.

At 100 hPa, as indicated by Figure 2, more evident seasonal variations of temperature can be seen in the tropics, with similar amplitude to that in mid-latitudes of both hemispheres. Compared with the GNSS RO temperature, ERA-I shows evident cold bias in the tropics during the period 2002-2006. For ERA5, such bias is largely corrected. For the later period 2007-2017, the differences between three reanalyses and the GNSS RO are comparable in magnitude, although the ERA5 shows slightly better agreement with GNSS RO measurements. In mid-latitudes of both hemispheres, very similar characteristics can be seen through the three reanalyses, which show slightly better agreement with the GNSS RO than in the tropics. However, relatively large bias can still be seen in the early stage from 2002 to 2006.

Temperature in the lower stratosphere (70 hPa) shows clear annual cycle in the tropics (figure 3(a)). However, the annual minimum and maximum values vary year-to-year, which indicate influences from the QBO. Large sub-seasonal fluctuations of temperature can be seen in mid-latitude of the NH, which is obviously different from that in the SH. That is related to strong equatorial as well as extra-tropical wave activities in this region. Again, large differences up to 1 K exists between the reanalyses and the GNSS RO observations during the first stage 2002-2006. ERA5 shows obvious cold bias in all selected regions while MERRA2 is anomalously warmer than the GNSS RO in mid-latitudes of both hemispheres. ERA-I, however, has no consistent warm or cold bias and shows the best agreement with the GNSS RO for the period 2002-2006. For the latter stage of 2007-2017, ERA5 shows the best agreement with observations (differences within 0.2 K) while the other two reanalyses are slightly (about 0.2 K) warm biased.

Note that the bias is particularly large during 2002-2006 for all reanalyses. This should be related to the assimilation of large number of COSMIC data since late 2006, which may cause sudden changes in reanalyses (Sturaro, 2003; Sterl, 2004). At the same time, the GNSS RO data could be also affected by the transition from the single CHAMP satellite to six COSMIC satellites since late 2006. To quantify the sampling errors and bias between two RO missions, we compared COSMIC and CHAMP monthly means for their overlap period of Jun. 2006-Sep. 2008. In addition, the lapse rate tropopause is calculated using the GNSS RO data with the method described in Fueglistaler et al. (2009) and shown in figure 4(a). Figure 4(b) shows that COSMIC monthly zonal mean temperatures are consistent colder (0.1-0.2 K) than CHAMP in the stratosphere. The cold is consistent with previous studies (Foelsche et al., 2008; Ho et al., 2009), although the differences between CHAMP and COSMIC are slightly larger than 0.1 K in some areas in the middle stratosphere (50-10 hPa). According to Schrøder et al. (2007); Leroy et al. (2018) the cold bias between CHAMP and COSMIC is the consequence of a change in the signal-to-noise ratio from 550 in CHAMP to 700 in COSMIC. In addition, the ribbed pattern in the meridional structure of the bias in the figure 4 is a consequence of sampling error (Leroy et al., 2018). The bias between COSMIC and CHAMP was computed from the 28-month period of overlap and removed from CHAMP-retrieved temperature for the further analysis in this work.

Figure 5 shows differences between three reanalyses and the corrected CHAMP for the period 2002-2006 and COSMIC for the period 2007-2017, respectively. For the first stage, MERRA2 shows warm bias of 0.1-0.2 K in the upper troposphere, cold bias of 0.1-0.3 K in the lower stratosphere and warm bias of 0.1-0.5 K in the middle stratosphere. ERA5 shows relatively small cold bias of 0.1-0.2 K for almost the whole UTLS region. ERA-I shows warm bias of 0.1-0.3 K in the upper troposphere and cold bias of 0.1-0.4 K in the middle stratosphere in both tropics and SH. For the second stage, differences between all three reanalysis and the GNSS RO are much smaller. That is because the reanalyses are better constrained by large number of COSMIC measurements. MERRA2 shows differences with GNSS RO less than 0.1 K except that cold bias of about 0.2 K at 10 hPa and northern mid-latitudes at 200-250 hPa. ERA5 shows perfect agreement to the COSMIC with differences less than 0.1 K in most of the UTLS region except that in northern mid-latitudes (100-50 hPa) with warm bias 0.1 K. Bias in ERA-I is also quite small with warm bias of about 0.1 K only in the tropics around the tropopause and southern mid-latitudes near 10 hPa.

In summary, reanalyses show very good agreement with the GNSS RO measurements in sub-seasonal to seasonal variations of temperature in the UTLS region. For the climatological values, a notable change around late 2006 can be found in all reanalyses. Relatively large bias of 0.1-0.5 K can be seen in MERRA2 and ERA-I for the first stage 2002-2006 while very good agreement can be seen between all reanalyses and the GNSS RO measurements for the 2007-2017. As the newest reanalysis, ERA5 shows relatively small bias of 0.1-0.3 K during 2002-2006 and has the best agreement with GNSS RO in general. To eliminate the effect of these discontinuities for further studies, reanalysis temperatures were corrected by using a transfer function approach similar to Wargan et al. (2018). The corrected GNSS RO temperature has no significant discontinuities and was used as a common baseline. Details of the bias correction for reanalysis temperatures are provided in the supplementary information (Figure S1).

3.2 Interannual Variability of temperature

Figure 6 shows one example of deseasonalized monthly anomalies of temperature in the tropical upper troposphere (10°S-10°N, at 150 hPa). As demonstrated in Figure 6a, temperature exhibits clear interannual variations, which is related to ENSO and QBO as indicated by previous studies (Randel and Wu, 2015). While the period of analysis is relatively short, such interannual fluctuations may significantly affect the calculation of linear trends. To estimate the influences of ENSO and QBO, a multiple linear regression method is applied as introduced in section 3.1. Figures 6d-f indicate contributions of QBO50, QBO30 and ENSO, respectively. ENSO contributes the largest and significant interannual variations of temperature in tropical upper troposphere with amplitude of about 0.5 K while QBO has only small and insignificant contributions. At lower levels in the free troposphere, the QBO contribution is smaller and the impacts of ENSO are more significant. Reanalyses reveal a very good agreement with each other as well as the GNSS RO in ENSO related contributions (Figure 6f) but show larger spread for QBO contributions. For the shorter period the interannual variability should have more influence on the trend calculations. By such a multiple linear regression, the influences of ENSO and QBO as well as the linear trend can be separated. Seen from Figure 6c, GNSS RO indicates an increase of 0.4 K in temperature for the whole period 2002-2017. The ERA-I trend is smallest (0.1 $\mathrm{K/decade}$). According to Simmons et al. (2014), local degradation occurs near the sub-tropical tropopause whereas substantial amounts of warm-biased aircraft data are assimilated since 1999. After 2006, while large number of COSMIC data is assimilated, this warm bias disappeared. This anomalous warm temperature for the short period 1999-2005 leads less warming in this region by estimated ERA-I time series. Such bias has been corrected in ERA5 temperature data. ERA5 shows obviously better agreement with GNSS RO.

In the lower stratosphere, as illustrated in Figure 7, interannual variations of temperature are dominated by QBO, with amplitudes of over 1 K for QBO50. The ENSO effects are insignificant with an amplitude of about 0.5 K. GNSS RO indicates an increase of 0.55 K as seen in Figure 7c. MERRA2 and ERA-I/ERA5 show similar increase of 0.65-0.7 K which is stronger than GNSS RO. The relative contributions of ENSO and QBO to interannual variations of zonal mean temperatures in the UTLS are shown in Figures 8-10.

Consistent with previous studies (Randel and Wu, 2015), positive ENSO is associated with warm temperature anomalies of 0.1-0.4 K in tropical upper troposphere and cold temperature anomalies of 0.1-0.5 K above the tropopause in the tropics (Figure 8). In contrast to the tropics, anomalous cold temperatures can be seen in the sub-tropics below 100 hPa while warm temperature anomalies exist above 100 hPa. All three reanalyses show consistent pattern as seen in GNSS RO associated with positive ENSO.

As a stratospheric phenomenon, westerly QBO affects the temperature mainly in the upper atmosphere above 100 hPa. The spatial structure of temperature anomalies associated with wind terms in m/s of QBO50 and QBO30 are shown in Figures 9-10. QBO50 is associated with warming in the lower most stratosphere (100-50 hPa) and cooling in middle stratosphere (50-15 hPa) in the tropics. Sub-tropics and mid-latitudes, however, show out-of-phase variations with significant warming signals. QBO30 contributes to similar temperature variations except that the signals are spatially orthogonal with the patterns associated

with QBO50 (Figure 10). Reanalyses show very good agreement with GNSS RO in both spatial pattern and magnitude for QBO related temperature variations as illustrated in Figures 9-10.

3.3 Temperature trends

Figure 11 summarize the spacial distribution of temperature trends based on corrected GNSS RO and reanalyses for the time period 2002-2017. From the GNSS RO measurements, positive trends of 0.2-0.3 $\mathrm{K/decade}$ are significant in most areas of the troposphere with stronger warming up to 0.4-0.5 $\mathrm{K/decade}$ in mid-latitudes of both hemispheres. At the same time, negative trends of 0.1-0.3 $\mathrm{K/decade}$ are evident in the stratosphere (50-10 hPa). In the lower most stratosphere (100-50 hPa), positive temperature trends are significant in the tropics. This is consistent with previous studies (Wang et al., 2013, 2015; Polvani et al., 2017), which indicated a warming in this region since 2001. However, the trends shown here (0.3 $\mathrm{K/decade}$ in maximum) are much smaller than that in their results (e.g., up to 1.6 $\mathrm{K/decade}$ in Wang et al. (2013)). Seen from the time series of temperature at 70 hPa (Figure 7), the temperature increases from 2002 until 2011 and then declines (or stop to increase) after that.

Reanalysis data show good agreement with the GNSS RO for the general pattern of temperature trends. However, slightly smaller trends are found in MERRA2 in the tropical free troposphere (400-200 hPa), which could be related to the observed warm bias during 2002-2006 in MERRA2 as illustrated in Figure 5. ERA-I shows neutral trends around 150-100 hPa in the tropics (15°S-15°N), which is positive by other data sets, which should be also related to the warm-biased aircraft data as mentioned in section 3.2. Very good agreement can be seen between ERA5 and the GNSS RO data in the troposphere with very similar spacial pattern and comparable magnitude of warm in the troposphere.

In the stratosphere, the negative trends in ERA-I are too weak and less significant in the SH. At the same time, positive trends in NH are stronger in both MERRA2 and ERA-I than that in GNSS RO. Again, ERA5 shows the best agreement with GNSS RO measurements with consistent pattern and comparable magnitude. At 10 hPa in the tropics, all the data sets show negative trends except ERA-I. According to Simmons et al. (2014), the large differences between MERRA2 and ERA-I at 10 hPa are associated with differing treatments of the change from SSU to AMSU-A and the availability of increasing amounts of largely unadjusted radiosonde data. While cell-pressure correction to SSU has been done in ERA5, it shows similar cooling trends to observations at 10 hPa. Also notable difference between GNSS RO and reanalyses can be seen in the tropics (5°S-20°N) around the lapse rate tropopause. Neutral trends are found by GNSS RO and ERA-I in this region, while ERA5 shows insignificant positive trends (0.2 $\mathrm{K/decade}$) and MERRA2 shows insignificant negative trends (-0.1 $\mathrm{K/decade}$). As a transition zone between the troposphere and the stratosphere, opposite sign could appear in neighboring layers below or above the tropopause, which causes large uncertainties in estimated trends around the tropopause.

Figure 12 further illustrates the temperature trends based on uncorrected/corrected GNSS RO and reanalysis data sets in three regions (SM: 25°S-45°S; NM: 25°N-45°N; TP: 10°S-10°N) at selected pressure levels (250, 150, 70, 50, 20, 10 hPa). The temperature increase in the upper troposphere is stronger and the cooling in the stratosphere gets weaker after the correction of the GNSS RO data. The differences of temperature trends between reanalysis and GNSS RO measurements become much smaller after corrections. For example, MERRA2 shows significant warming at 250 hPa in the SM after the correction, which is more consistent with the GNSS RO data. The unrealistic strong cooling in MERRA2 at 10 hPa is significantly reduced by the

correction. Overall, the reanalysis data represent the temperature trends well from the upper troposphere to the mid-stratosphere after the correction, although obvious differences can be seen between reanalysis and the GNSS RO measurements. As the newest reanalysis, ERA5 shows the best agreement with the GNSS RO measurements among most of areas as demonstrated in this study.

Note that the temperature trends discussed above are based on a relatively short data record of 16 years. The statistically significance of the obtained trends must be specially concerned since the trend assessment from such a short period can be strongly influenced by start/end years (Bandoro et al., 2018; Santer et al., 2017). Beside the two-sided Student's t test as mentioned in section 2.5, a signal-to-noise study is also included. The background noise of 16-year temperature trends are estimated by three fully coupled CESM simulations, which were integrated 145 years (1955 to 2099) with anthropogenic emissions (GHGs and ODSs) fixed to values at 1960. We fit linear trends to overlapping 192-month segments of the 1740-month in each of CESM runs and then the noise can be calculated by the standard deviation of the 16-year trends. More details of the CESM simulations and the methods can be seen in the supplements. The signal to noise ratios of 16-year GNSS RO temperature trends are shown in Fig. S2. Seen from Fig. S2, the areas with significant trends are smaller than that shown in Figure 11 in the main text. However, there are still significant signals in the mid-latitudes of the upper troposphere, around the tropopause and in the SH in the middle stratosphere. All the significant regions in Figure S2 are actually the most important areas with strongest and significant trends in Figure 11. This suggests that the significant trends shown in Figure 11 are robust except that in the tropics whereas the standard deviation of the trends are the strongest.

To explain the underlying mechanisms such as dynamical processes associated with SST of the illustrated temperature trends, two WACCM simulations as described in section 2.4 were employed. Figure 13 shows the temperature trends from the Transient run and the FixSST run as well as their differences. The Transient run with varying SST (Figure 13a) shows comparable positive trends (0.2-0.3 $\mathrm{K/decade}$) in the troposphere and negative trends (0.1-0.5 $\mathrm{K/decade}$) in the stratosphere (see Figure 11 for a comparison). While the SSTs are fixed to climatological values, which means only radiative effects from GHGs and ODSs are included, the positive trends in the troposphere disappear or become much weaker (Figure 13b). This reveals that the influences of SSTs on circulation are the main reason for the warming temperature trends in troposphere, which can be confirmed by the differences between these two runs (Figure 13c). The negative temperature trends in the stratosphere (tropics and SH) persist in the FixSST run, which illustrates other factors like radiative effects from GHGs and ozone contribute to such cooling. For the temperature trends above the tropical tropopause (100-50 hPa), the weak warming is related to combined effects of SSTs (contribute to a cooling) and other effects (lead to a warming).

3.4 Coupling with ozone

Figure 14 shows the initial ozone time series from the SWOOSH, C3S, MERRA2 and ERA5 as well as their differences using the SWOOSH data as a reference in three regions at 70 hPa. The ERA-I is not included here for ozone analysis because it does not assimilate as many ozone measurements as ERA5 and MERRA2. Although the phase and amplitude agree well in general, the absolute ozone values have large differences between different data sets. Obvious missing data and extreme values exist in both SWOOSH and C3S data sets during 2002-2004, while a discontinuity in the MERRA2 and ERA5 time series occurs

in mid-2004 when Aura MLS mission starts. As illustrated in Figure 14, extreme large values are observed by SWOOSH and C3S around 2003. The reason is the limited number of observation in this period, which could cause large sampling errors and uncertainties in ozone data. At the same time, since the reanalysis is less constrained during this period, large bias can be seen in both MERRA2 and ERA5 compared to observations (Figures 14b, d and f). After 2006, SWOOSH uses MLS ozone data only (Davis et al., 2016) and MERRA2 also uses MLS instead of SBUV ozone data since Oct. 2004 (Gelaro et al., 2017). Therefore the MERRA2 ozone data have good agreement with SWOOSH data. Another discontinuity in the MERRA2 and ERA5 time series occurs around 2015. According to McCarty et al. (2016), MERRA2 starts to use the version 4.2 MLS ozone data instead of version 2.2 since June 2015, which cause data discontinuities at 250-70 hPa. As seen in Figures 14b, d and f, ozone in MERRA2 is 50-150 ppbv lower than that in SWOOSH and C3S. ERA5 combined more satellite data (SBUV and MLS) than MERRA2, which leads to larger variability of ozone in ERA5 since the different data sets and different ways for merging the data have large influences on the ozone data. The missing data and extreme values in SWOOSH and C3S, as well as the data discontinuities in MERRA2 and ERA5 around years 2004 and 2015 can also be seen at other pressure levels (See Figures S3-S4 for details).

To examine the connection between the vertical temperature changes and ozone distribution, ozone trends are analyzed in the stratosphere from 250 to 10 hPa. In consideration of the discontinuities in MERRA2 and ERA5 around late 2004 due to the MLS ozone data, a step-function proxy is added for the Jan. 2002-Sep. 2004 in the trend calculation. An extra step-function proxy is added in the MERRA2 MLR to remove the discontinuities associated with the transition from MLS v2.2 to v4.2 for 250-70 hPa for the period Jun. 2015-Dec. 2017. The trends are calculated for the period 2002-2017 using the same MLR method as for temperature but with step function proxies in the reanalyses (Figure 15). SWOOSH and C3S ozone trends show good agreement in spacial distribution as well as magnitude in general (Figures 15a and b). From 250 to 100 hPa, ozone trends are mainly insignificant or opposite in sign by different data sets due to the large uncertainties of ozone data in this region. Asymmetry trends in two hemispheres, with significant decrease of ozone in NH mid-latitudes at 100-10 hPa and increase of ozone in SH mid-latitudes are found at 50-10 hPa. This is consistent with a recent study using the MLS ozone data (Chipperfield et al., 2018). At 100-50 hPa, ozone is decreasing in NH mid-latitudes based on satellite data but positive or insignificant trend by reanalysis data. Stonger positive trends in tropics and SH mid-latitudes and less negative trends in NH mid-latitudes are found by ERA5 data at 30-20 hPa, which is related to the positive ERA5 bias during 2015-2017 in these regions (Figures S4).

Figure 16 shows the ozone trends from two model simulations as well as their differences. The ozone trends based on the model simulation with varying SST show similar trends as SWOOSH and C3S data. Insignificant trends are found at 250-100 hPa in most regions. The maximum negative trends (-100 ppbv/decade) located around 25-20 hPa in NH mid-latitudes while the maximum positive trends at 10 hPa in tropics. While the SSTs are fixed to climatological values, ozone increases from the tropics to SH mid-latitudes in the middle stratosphere (30-10 hPa) and negative trends in the NH mid-latitudes from 100 to 10 hPa become much weaker (Figure 16b). The differences between these two runs, which indicate contributions from SSTs, show similar spacial pattern with the Transient run as well as observations. This confirms that dynamic processes are dominated for ozone trends in the middle stratosphere (100-10 hPa in NH and 30-20 hPa in tropics), which is consistent with

the previous study (Chipperfield et al., 2018). For the tropical lower stratosphere (20°S-20°N, 70-30 hPa), ozone trends are determined by a combination of ODSs and SSTs (Figures 16b-c).

Considering the coupling between changes in ozone and temperature, the correlation coefficients between ozone and temperature anomalies for the period 2002-2017 are calculated. Consistent with previous studies (Abalos et al., 2012; Maycock, 2016; Gilford et al., 2016), observed ozone (GNSS RO) and temperature (SWOOSH) anomalies are highly correlated (>0.6) in the range from 100 to 20 hPa (Figure S5a). The correlation coefficients are highest in tropical region ($\sim$0.9). MERRA2 shows a similar correlation between ozone and temperature while the correlation in ERA5 is slightly weaker. Furthermore, we estimate a factor $b_f(p)$ between temperature and ozone anomalies at each grid point p by linear regression:

$$y(p,t) = b_f(p) \cdot x(p,t) \tag{2}$$

where $y(p,t)$ is monthly temperature anomalies and $x(p,t)$ is the monthly ozone anomalies at each grid point p. Then the potential contribution of ozone changes to temperature trends $T(p)$ are estimated by the ozone trend $O_3(p)$ and $b_f(p)$ with Eq. 3 (Figure 16d and Figure S6d).

$$T(p) = O_3(p) \cdot b_f(p) \tag{3}$$

While ozone and temperature are positively correlated, a decrease of ozone contributes to a cooling in the NH and in the tropical upper troposphere and mid-stratosphere. Increases of ozone lead to a warming effect in the SH and the lower stratosphere in the tropics.

Recall the question of the temperature trend attribution, the positive trends in the upper troposphere can be well explained by increases in SSTs (Figure 13). The stratospheric cooling, however, can not be fully explained. Satellite measurements show a stronger cooling in the SH than that in the NH. Model simulation and ozone-temperature correlations indicate that both SST and ozone changes contribute to a cooling in the NH but a warming in the SH. The exact reason for the strong cooling in the lower to mid-stratosphere in the SH awaits further studies. For the tropical warming in the lower stratosphere, it is related to both SST and ozone changes. As seen in Figure S6 SSTs are significantly increased during 2002-2017 almost globally except in the North Atlantic and the Southern Ocean. Such increase in SSTs would warm up the troposphere and lead to strengthening in upward motion of the atmosphere, which leads to a cooling in the tropical lower stratosphere. At the same time, ozone is increased and contributes to a warming in that region (Figures 16 and S5) . As indicated by Wang et al. (2015), the increase of temperature in the tropical lower stratosphere is dominated by an anomalous SST decline from 2001 to 2011. While a significant increase of SST occurs after 2011, the temperature in the tropical lower stratosphere decreases and leads to a net cooling for the period 2002-2017. Ozone increases from 2002 to 2017 and contributes to a warming effect to the tropical lower stratosphere. However, the potential contribution of ozone to temperature in the tropical lower stratosphere is quite weak, which can not fully explain the observed warming in that region.

4 Conclusions and Discussion

The recent variability and trends of temperature in the UTLS have been studied for the period 2002-2017 using the high quality, high vertical resolution GNSS RO data. The newest ERA5 reanalysis product, as well as the MERRA2 and the ERA-I reanalyses are evaluated for seasonal-to-interannual variations as well as linear trends of temperature in the UTLS.

In general, all three reanalyses show good agreement with the GNSS RO measurements for the annual cycle of temperature with consistent phase and comparable amplitude. However, relative large biases can be seen between reanalysis data set and GNSS RO for the period 2002-2006, which reveals an evident discontinuity of temperature time series in reanalyses. That is caused by the lack of observations and less constrained reanalysis data in the first stage and large amounts of data from the COSMIC satellite mission since 2007. Such discontinuity in reanalysis data should be carefully considered while using the reanalysis data analyzing trends. ERA5 shows obvious improvements of temperature data compared with ERA-I and also a slight better agreement with GNSS RO measurements than MERRA2.

Temperature in the UTLS presents significant interannual variations which has been well known that are related to ENSO and QBO. Based on a multiple linear regression method, the relative contributions of ENSO and a pair of orthogonal time series of QBO (QBO50 and QBO30) are estimated from the GNSS RO measurements as well as reanalysis data sets. Signals of ENSO and QBO show very good agreement between all three reanalyses and the GNSS RO data, which indicates that the reanalyses are able to capture interannual variations of temperature in the UTLS.

16 years of temperature data were analyzed by a MLR method to determine trends in the UTLS. A significant warming of 0.2-0.3 $\mathrm{K/decade}$ can be seen in most areas of the troposphere with stronger increase of 0.4-0.5 $\mathrm{K/decade}$ in mid-latitudes of both hemispheres. Contrast to the troposphere, the stratospheric temperature decreases at a rate of 0.1-0.3 $\mathrm{K/decade}$. Positive temperature trends are significant in the tropical lower stratosphere (100-50 hPa) with a much weaker magnitude (0.1-0.5 $\mathrm{K/decade}$) than that in a former period (2001-2011) as shown by a previous study (Wang et al., 2015). Again, ERA5 shows improved quality compared with ERA-I and has the best agreement with the GNSS RO data in the three reanalyses. MERRA2 shows less significant warming trends in the tropical troposphere and too strong cooling in its initial data but more consistent trends after the discontinuity corrections.

Similar with temperature data, reanalysis ozone are affected by the change of assimilated observations and methods. Negative trends of ozone are dominated in the NH at 150-50 hPa. In the tropical lower stratosphere, increases of ozone are evident. Asymmetric trends of ozone can be found for the two hemispheres in the middle stratosphere, with significant ozone decrease in NH mid-latitudes and increases of ozone in SH mid-latitudes. Around the tropopause, trends are small and large differences between data sets are found. Further study and longer time series are needed for trend analyses in these regions. Overall, large biases exist in reanalysis and it is still challenging to do trend analysis based on reanalysis ozone data.

According to model simulations, the temperature increase in the troposphere as well as ozone decrease in the NH stratosphere could be mainly connected to the increase of SST and subsequent changes of atmospheric circulations. Ozone increases around 20 hPa in the SH, decreases around 30 hPa and increases from 20 to 10 hPa in the tropics are also closely related to SST changes. This supports the results of Chipperfield et al. (2018) which concluded that dynamical changes play an important

role for the ozone variability in the stratosphere. Ozone increases in the tropical lower stratosphere may related to reduced emissions of ODSs since the Montreal Protocol (Polvani et al., 2017), and are partly offset by SST changes.

In the stratosphere, ozone and temperature variations are highly correlated with each other. Due to the radiative effects of ozone, a decrease of ozone in the NH contributes partly to the temperature decrease in this region. The increased ozone may contribute to the temperature increase in the tropical lower stratosphere. However, this contribution from ozone is relateively weak and can not fully explain the warming in that regions. In addition, it is partly offset by the cooling effect of increases in SSTs. The long-term trend of temperature in the lower stratosphere is strongly modified by interannual and decadal fluctuations related to natural processes like SST variations.

Recent temperature and ozone trends have been calculated by a MLR method based on observational data sets. However, trend assessments over short period of 1-2 decades are largely uncertain since the calculated trends are sensitive to start or end date (Santer et al., 2017). As RO data are acquired over longer periods with large number of observations (more than 10000 per day) by COSMIC2, the climate signal will emerge robustly and be more reliable for the temperature trends and variability studies in the UTLS.

Author contributions. M. Shangguan performed the computational implementation and the analysis, created the figures, and wrote the first draft of the paper. All authors contributed to the study design. W. Wang made the model simulations and provided advice on the analysis design and contributed to the text. S. Jin contributed to the text.

Acknowledgements. This work was supported jointly by the Natural Science Foundation of Jiangsu Province (BK20170665), the National Natural Science Foundation of China (41705023) and the Postdoctoral Science Foundation of China (2017M610319).The numerical calculations in this paper have been done on the computing facilities in the High Performance Computing Center (HPCC) of Nanjing University. We thank CDAAC for the use of the COSMIC GNSS RO data sets, the NOAA for QBO and MEI data, the ECMWF for the ERA-Interim and ERA5 data, the NASA GSFC for MERRA2 data, the NOAA Chemical Sciences Division for the SWOOSH data and Copernicus Climate Change Service for SAGE-II/CCI/OMPS ozone products.

References

Abalos, M., Randel, W. J., and Serrano, E.: Variability in upwelling across the tropical tropopause and correlations with tracers in the lower stratosphere, Atmospheric Chemistry and Physics, 12, 11 505–11 517, https://doi.org/10.5194/acp-12-11505-2012, https://www.atmos-chem-phys.net/12/11505/2012/, 2012.

Anthes, R. A., Bernhardt, P. A., Chen, Y., Cucurull, L., Dymond, K. F., Ector, D., Healy, S. B., Ho, S. P., Hunt, D. C., and Kuo, Y.-H.: The COSMIC/FORMOSAT-3 Mission: Early Results, Bulletin of the American Meteorological Society, 89, 313–333, 2008.

Ball, W. T., Alsing, J., Mortlock, D. J., Staehelin, J., Haigh, J. D., Peter, T., Tummon, F., Stübi, R., Stenke, A., Anderson, J., Bourassa, A., Davis, S. M., Degenstein, D., Frith, S., Froidevaux, L., Roth, C., Sofieva, V., Wang, R., Wild, J., Yu, P., Ziemke, J. R., and Rozanov, E. V.: Evidence for a continuous decline in lower stratospheric ozone offsetting ozone layer recovery, Atmospheric Chemistry and Physics, 18, 1379–1394, https://doi.org/10.5194/acp-18-1379-2018, 2018.

Bandoro, J., Solomon, S., Santer, B. D., Kinnison, D. E., and Mills, M. J.: Detectability of the impacts of ozone-depleting substances and greenhouse gases upon stratospheric ozone accounting for nonlinearities in historical forcings, Atmospheric Chemistry and Physics, 18, 143–166, https://doi.org/10.5194/acp-12-11505-2012, 2018.

Chipperfield, M. P., Dhomse, S., Hossaini, R., W., F., Santee, M., Weber, M., Burrows, J. P., Wild, J., Loyola, D., and Coldewey-Egbers, M.: On the Cause of Recent Variations in Lower Stratospheric Ozone, Geophysical Research Letters, 45, 1–9, 2018.

Davis, S. M., Rosenlof, K. H., Hassler, B., Hurst, D. F., Read, W. G., Vömel, H., Selkirk, H., Fujiwara, M., and Damadeo, R.: The Stratospheric Water and Ozone Satellite Homogenized (SWOOSH) database: a long-term database for climate studies, Earth System Science Data, 8, 461–490, https://doi.org/10.5194/essd-8-461-2016, 2016.

Davis, S. M., Hegglin, M. I., Fujiwara, M., Dragani, R., Harada, Y., Kobayashi, C., Long, C., Manney, G. L., Nash, E. R., and Potter, G. L.: Assessment of upper tropospheric and stratospheric water vapor and ozone in reanalyses as part of S-RIP, Atmospheric Chemistry & Physics, 17, 1–57, 2017.

Dee, D. P., Uppala, S. M., Simmons, A. J., Berrisford, P., Poli, P., Kobayashi, S., Andrae, U., Balmaseda, M. A., Balsamo, G., and Bauer, P.: The ERA-Interim reanalysis: configuration and performance of the data assimilation system, Quarterly Journal of the Royal Meteorological Society, 137, 553–597, 2011.

Dragani, R.: On the quality of the ERA-Interim ozone reanalyses: comparisons with satellite data, Quarterly Journal of the Royal Meteorological Society, 137, 1312–1326, https://doi.org/https://doi.org/10.1002/qj.821, 2011.

Flato, G., Marotzke, J., Abiodun, B., Braconnot, P., Chou, S, C., Collins, W., Cox, P., Driouech, F., Emori, S., Eyring, V., Forest, C., Gleckler, P., Guilyardi, E., Jakob, C., Kattsov, V., Reason, C., and Rummukainen, M.: Evaluation of Climate Models, in: Climate Change 2013 - The Physical Science Basis. Contribution of Working Group I to the Fifth Assessment Report of the Intergovernmental Panel on Climate Change [Stocker, T.F., D. Qin, G.-K. Plattner, M. Tignor, S.K. Allen, J. Boschung, A. Nauels, Y. Xia, V. Bex and P.M. Midgley (eds.)], pp. 741–866, Cambridge University Press, Cambridge, United Kingdom and New York, NY, USA, http://dx.doi.org/10.1017/CBO9781107415324.020, 2014.

Foelsche, U., Borsche, M.and Steiner, A. K., Gobiet, A., Pirscher, B., Kirchengast, G., Wickert, J., and Schmidt, T.: Observing upper troposphere–lower stratosphere climate with radio occultation data from the CHAMP satellite, Climate Dynamics, 31, 49–65, 2008.

Forster, P. M., Bodeker, G., Schofield, R., Solomon, S., and Thompson, D.: Effects of ozone cooling in the tropical lower stratosphere and upper troposphere, Geophysical Research Letters, 34, https://doi.org/10.1029/2007GL031994, 2007.

Fueglistaler, S., Dessler, A., Dunkerton, T., Folkins, I., Fu, Q., and Mote, P. W.: Tropical tropopause layer, Reviews of Geophysics, 47, 1004, https://doi.org/10.1029/2008RG000267, 2009.

Fueglistaler, S., Abalos, M., Flannaghan, T. J., Lin, P., and Randel, W. J.: Variability and trends in dynamical forcing of tropical lower stratospheric temperatures, Atmospheric Chemistry and Physics, 14, 13 439–13 453, https://doi.org/10.5194/acp-14-13439-2014, 2014.

Garfinkel, C. I., Gordon, A., Oman, L. D., Li, F., Davis, S., and Pawson, S.: Nonlinear response of tropical lower-stratospheric temperature and water vapor to ENSO, Atmospheric Chemistry and Physics, 18, 4597–4615, https://doi.org/10.5194/acp-18-4597-2018, 2018.

Gelaro, R., Mccarty, W., Suárez, M. J., Todling, R., Molod, A., Takacs, L., Randles, C. A., Darmenov, A., Bosilovich, M. G., and Reichle, R.: The Modern-Era Retrospective Analysis for Research and Applications, Version 2 (MERRA-2), Journal of Climate, 30, 2017.

Gettelman, A. and Birner, T.: Insights into tropical tropopause layer processes using global models, Journal of Geophysical Research Atmospheres, 112, D23 104, https://doi.org/10.1029/2007JD008945, 2007.

Gilford, D. M., Solomon, S., and Portmann, R. W.: Radiative Impacts of the 2011 Abrupt Drops in Water Vapor and Ozone in the Tropical Tropopause Layer, Journal of Climate, 29, 595–612, https://doi.org/10.1175/JCLI-D-15-0167.1, 2016.

Harris, N. R. P., Hassler, B., Tummon, F., Bodeker, G. E., Hubert, D., Petropavlovskikh, I., Steinbrecht, W., Anderson, J., Bhartia, P. K., Boone, C. D., Bourassa, A., Davis, S. M., Degenstein, D., Delcloo, A., Frith, S. M., Froidevaux, L., Godin-Beekmann, S., Jones, N., Kurylo, M. J., Kyrölä, E., Laine, M., Leblanc, S. T., Lambert, J.-C., Liley, B., Mahieu, E., Maycock, A., de Mazière, M., Parrish, A., Querel, R., Rosenlof, K. H., Roth, C., Sioris, C., Staehelin, J., Stolarski, R. S., Stübi, R., Tamminen, J., Vigouroux, C., Walker, K. A., Wang, H. J., Wild, J., and Zawodny, J. M.: Past changes in the vertical distribution of ozone – Part 3: Analysis and interpretation of trends, Atmospheric Chemistry and Physics, 15, 9965–9982, https://doi.org/10.5194/acp-15-9965-2015, 2015.

Ho, S. P., Kirchengast, G., Leroy, S., Wickert, J., Mannucci, A. J., Steiner, A., Hunt, D., Schreiner, W., Sokolovskiy, S., Ao, C., Borsche, M., Engeln, A. v., Foelsche, U., Heise, S., Iijima, B., Kuo, Y., Kursinski, R., Pirscher, B., Ringer, M., Rocken, C., and Schmidt, T.: Estimating the uncertainty of using GPS radio occultation data for climate monitoring: Intercomparison of CHAMP refractivity climate records from 2002 to 2006 from different data centers, Journal of Geophysical Research Atmospheres, 114, https://doi.org/10.1029/2009JD011969, 2009.

Ho, S. P., Hunt, D., Steiner, A. K., Mannucci, b. J., Kirchengast, G., Gleisner, H., Heise, S., Engeln, A. v., Marquardt, C., Sokolovskiy, S., Schreiner, W., Scherllin-Pirscher, B., Ao, C., Wickert, J., Syndergaard, S., Lauritsen, K. B., Leroy, S., Kursinski, E. R., Kuo, Y. H., Foelsche, U., Schmidt, T., and Gorbunov, M.: Reproducibility of GPS radio occultation data for climate monitoring: Profile-to-profile inter-comparison of CHAMP climate records 2002 to 2008 from six data centers, Journal of Geophysical Research Atmospheres, 117, https://doi.org/10.1029/2012JD017665, 2012.

Ho, S. P., Peng, L., and Vömel, H.: Characterization of the long-term radiosonde temperature biases in the upper troposphere and lower stratosphere using COSMIC and Metop-A/GRAS data from 2006 to 2014, Atmospheric Chemistry & Physics, pp. 1–58, 2016.

Kim, J., Grise, K. M., and Son, S. W.: Thermal characteristics of the cold-point tropopause region in CMIP5 models, J. Geophys. Res., 118, 8827–8841, https://doi.org/10.1002/jgrd.50649, 2013.

Kuleshov, Y., Choy, S.and Fu, E. F., Chane-Ming, F., Liou, Y. A., and Pavelyev, A. G.: Analysis of meteorological variables in the Australasian region using ground- and space-based GPS techniques, Atmospheric Research, 176-177, 276–289, 2016.

Kuo, Y.-H., Wee, T.-K., Sokolovskiy, S., Rocken, C., Schreiner, W., Hunt, D., and Anthes, R. A.: Inversion and Error Estimation of GPS Radio Occultation Data, Journal of the Meteorological Society of Japan. Ser. II, 82, 507–531, https://doi.org/10.2151/jmsj.2004.507, 2004.

Ladstädter, F., Steiner, A. K., Foelsche, U., Haimberger, L., Tavolato, C., and Kirchengast, G.: An assessment of differences in lower stratospheric temperature records from (A)MSU, radiosondes, and GPS radio occultation, Atmospheric Measurement Techniques, 4, 1965–1977, https://doi.org/10.5194/amt-4-1965-2011, 2011.

Leroy, S. S., Ao, C. O., and Verkhoglyadova, O. P.: Temperature Trends and Anomalies in Modern Satellite Data: Infrared Sounding and GPS Radio Occultation, Journal of Geophysical Research Atmospheres, https://doi.org/10.1029/2018JD028990, 2018.

Marsh, D. R., Mills, M. J., Kinnison, D. E., Lamarque, J. F., Calvo, N., and Polvani, L. M.: Climate Change from 1850 to 2005 Simulated in CESM1(WACCM), Journal of Climate, 26, 7372–7391, 2013.

Matthes, K., Marsh, D. R., Garcia, R. R., Kinnison, D. E., Sassi, F., and Walters, S.: Role of the QBO in modulating the influence of the 11 year solar cycle on the atmosphere using constant forcings, Journal of Geophysical Research Atmospheres, 115, 18 110, https://doi.org/10.1029/2009JD013020, 2010.

Maycock, A. C.: The contribution of ozone to future stratospheric temperature trends, Geophysical Research Letters, 43, https://doi.org/10.1002/2016GL068511, 2016.

McCarty, W., Coy, L., Gelaro, R., Huang, A., Merkova, D., Smith, E. B., Sienkiewicz, M., and K., W.: NASA Tech. Rep. NASA/TM–2016–104606, https://gmao.gsfc.nasa.gov/pubs/docs/McCarty885.pdf, 2016.

Modeling, G. and Office, A.: MERRA2 instM_3d_ana_Np: 3d, monthly mean,instantaneous,pressure-level,analysis,analyzed meteorological fields V5.12.4,Greenbelt, MD, USA, Goddard Earth Sciences Data and Information Services Center (GES DISC), Accessed: October 2018, https://doi.org/10.5067/V92O8XZ30XBI, 2015.

Pirscher, B., Foelsche, U., Lackner, B. C., and Kirchengast, G.: Local time influence in single-satellite radio occultation climatologies from Sun-synchronous and non-Sun-synchronous satellites, Journal of Geophysical Research Atmospheres, 112, 2007.

Polvani, L. M. and Solomon, S.: The signature of ozone depletion on tropical temperature trends, as revealed by their seasonal cycle in model integrations with single forcings, Journal of Geophysical Research Atmospheres, 117, https://doi.org/10.1029/2012JD017719, 2012.

Polvani, L. M., Wang, L., Aquila, V., and Waugh, D. W.: The impact of ozone-depleting substances on tropical upwelling, as revealed by the absence of lower-stratospheric cooling since the late 1990s, Journal of Climate, 30, 2523–2534, https://doi.org/10.1175/JCLI-D-16-0532.1, 2017.

Randel, W. J. and Wu, F.: Variability of zonal mean tropical temperatures derived from a decade of GPS radio occultation data, J. Atmos. Sci., 72, 1261–1275, https://doi.org/10.1175/JAS-D-14-0216.1, 2015.

Randel, W. J., Shine, K. P., Austin, J., Barnett, J., Claud, C., Gillett, N. P., Keckhut, P., Langematz, U., Lin, R., and Long, C.: An update of observed stratospheric temperature trends, Journal of Geophysical Research Atmospheres, 114, 356–360, 2009.

Randel, W. J., Polvani, L., Wu, F., Kinnison, D. E., Zou, C. Z., and Mears, C.: Troposphere-stratosphere temperature trends derived from satellite data compared with ensemble simulations from WACCM: Satellite vs. modeled temperature trends, Journal of Geophysical Research Atmospheres, 122, https://doi.org/10.1002/2017JD027158, 2017.

Rayner, N. A., Parker, D. E., Horton, E. B., Folland, C. K., Alexander, L. V., Rowell, D. P., Kent, E. C., and Kaplan, A.: Global analyses of sea surface temperature, sea ice, and night marine air temperature since the late nineteenth century, J. Geophys. Res., 108, 4407–4453, https://doi.org/10.1029/2002JD002670, 2003.

Santer, B. D., Solomon, S., Wentz, F. J., Fu, Q., Po-Chedley, S., Mears, C., Painter, J. F., and Bonfils, C.: Tropospheric Warming Over The Past Two Decades:, Scientific Reports, 7, 2336, 2017.

Scherllin-Pirscher, B., Steiner, A. K., Kirchengast, G., Kuo, Y.-H., and Foelsche, U.: Empirical analysis and modeling of errors of atmospheric profiles from GPS radio occultation, Atmospheric Measurement Techniques, 4, 1875–1890, https://doi.org/10.5194/amt-4-1875-2011, 2011.

Schmidt, T., Wickert, J., Beyerle, G., König, R., Galas, R., and Reigber, C.: The CHAMP Atmospheric Processing System for Radio Occultation Measurements, Springer Berlin Heidelberg, 2005.

Schmidt, T., Wickert, J., and Haser, A.: Variability of the upper troposphere and lower stratosphere observed with GPS radio occultation bending angles and temperatures, Advances in Space Research, 46, 150–161, 2010.

Schoeberl, M. R., Douglass, A. R., Newman, P. A., Lait, L. R., Lary, D., Waters, J., Livesey, N., Froidevaux, L., Lambert, A., Read, W., Filipiak, M. J., and Pumphrey, H. C.: QBO and annual cycle variations in tropical lower stratosphere trace gases from HALOE and Aura MLS observations, Journal of Geophysical Research: Atmospheres, 113, https://doi.org/10.1029/2007JD008678, 2008.

Schrøder, T. M., Ao, C. O., and de la Torre JuáRez, M.: Sensitivity of GPS occultation to the stratopause height, Journal of Geophysical Research Atmospheres, 112, D06 119, https://doi.org/10.1029/2006JD007330, 2007.

Simmons, A. J., Poli, P., Dee, D. P., Berrisford, P., Hersbach, H., Kobayashi, S., and Peubey, C.: Estimating low-frequency variability and trends in atmospheric temperature using ERA-Interim, Quarterly Journal of the Royal Meteorological Society, 140, 329–353, 2014.

Sofieva, V. F., Kyrölä, E., Laine, M., Tamminen, J., Degenstein, D., Bourassa, A., Roth, C., Zawada, D., Weber, M., Rozanov, A., Rahpoe, N., Stiller, G., Laeng, A., von Clarmann, T., Walker, K. A., Sheese, P., Hubert, D., van Roozendael, M., Zehner, C., Damadeo, R., Zawodny, J., Kramarova, N., and Bhartia, P. K.: Merged SAGE II, Ozone_cci and OMPS ozone profile dataset and evaluation of ozone trends in the stratosphere, Atmospheric Chemistry and Physics, 17, 12 533–12 552, https://doi.org/10.5194/acp-17-12533-2017, 2017.

Staten, P. W. and Reichler, T.: Use of radio occultation for long-term tropopause studies: Uncertainties, biases, and instabilities, Journal of Geophysical Research Atmospheres, 113, 2008.

Steinbrecht, W., Froidevaux, L., Fuller, R., Wang, R., Anderson, J., Roth, C., Bourassa, A., Degenstein, D., Damadeo, R., Zawodny, J., Frith, S., McPeters, R., Bhartia, P., Wild, J., Long, C., Davis, S., Rosenlof, K., Sofieva, V., Walker, K., Rahpoe, N., Rozanov, A., Weber, M., Laeng, A., von Clarmann, T., Stiller, G., Kramarova, N., Godin-Beekmann, S., Leblanc, T., Querel, R., Swart, D., Boyd, I., Hocke, K., Kämpfer, N., Maillard Barras, E., Moreira, L., Nedoluha, G., Vigouroux, C., Blumenstock, T., Schneider, M., García, O., Jones, N., Mahieu, E., Smale, D., Kotkamp, M., Robinson, J., Petropavlovskikh, I., Harris, N., Hassler, B., Hubert, D., and Tummon, F.: An update on ozone profile trends for the period 2000 to 2016, Atmospheric Chemistry and Physics, 17, 10 675–10 690, https://doi.org/10.5194/acp-17-10675-2017, 2017.

Sterl, A.: On the (In)Homogeneity of Reanalysis Products., Journal of Climate, 17, 3866–3873, 2004.

Sturaro, G.: A closer look at the climatological discontinuities present in the NCEP/NCAR reanalysis temperature due to the introduction of satellite data, Climate Dynamics, 21, 309–316, 2003.

Trenberth, K. E. and Smith, L.: The Vertical Structure of Temperature in the Tropics: Different Flavors of El Niño, Journal of Climate, 19, 4956, 2006.

Trenberth, K. E. and Smith, L.: Variations in the three-dimensional structure of the atmospheric circulation with different flavors of El Niño., Journal of Climate, 22, 2978–2991, 2009.

von Storch, H. and Zwiers, F. W.: Statistical analysis in climate research, Cambridge University Press, 2002.

Wang, J. S., Seidel, D. J., and Free, M.: How well do we know recent climate trends at the tropical tropopause?, J. Geophys. Res., 117, 09 118, https://doi.org/10.1029/2012JD017444, 2012.

Wang, W., Matthes, K., Schmidt, T., and Neef, L.: Recent variability of the tropical tropopause inversion layer, Geophysical Research Letters, 40, 6308–6313, 2013.

Wang, W., Matthes, K., and Schmidt, T.: Quantifying contributions to the recent temperature variability in the tropical tropopause layer, Atmospheric Chemistry & Physics, 15, 5815–5826, https://doi.org/10.5194/acp-15-5815-2015, 2015.

Wang, W., Matthes, K., Omrani, N.-E., and Latif, M.: Decadal variability of tropical tropopause temperature and its relationship to the Pacific Decadal Oscillation, Scientific Reports, 6, 29 537, https://doi.org/10.1038/srep29537, 2016.

Wargan, K., Labow, G., Frith, S., Pawson, S., Livesey, N., and Partyka, G.: Evaluation of the Ozone Fields in NASA's MERRA-2 Reanalysis, Journal of Climate, 30, 2961–2988, https://doi.org/10.1175/JCLI-D-16-0699.1, 2017.

Wargan, K., Orber, C., Pawson, S., Ziemke, J. R., Oman, L. D., Olsen, M. A., Coy, L., and Knowland, K. E.: Recent decline in extratropical lower stratospheric ozone attributed to circulation changes, Geophysical Research Letters, 45, 5166–5176, https://doi.org/10.1029/2018GL077406, 2018.

Wee, T.-K. and Kuo, Y.-H.: Advanced stratospheric data processing of radio occultation with a variational combination for multifrequency GNSS signals, Journal of Geophysical Research Atmospheres, 119, 11,011–11,039, 2015.

Wickert, J., Reigber, C., Beyerle, G.and König, R., Marquardt, C., Schmidt, T., Grunwaldt, L., Galas, R., Meehan, T. K., and Melbourne, W. G.: Atmosphere sounding by GPS radio occultation: First results from CHAMP, Geophysical Research Letters, 28, 3263–3266, 2001.

Xie, F., Li, J., Tian, W., Feng, J., and Huo, Y.: Signals of El Niño Modoki in the tropical tropopause layer and stratosphere, Atmospheric Chemistry and Physics, 12, 5259–5273, https://doi.org/10.5194/acp-12-5259-2012, 2012.

Zhao, Y. and Li, J.: Discrepancy of mass transport between the Northern and Southern Hemispheres among the ERA-40, NCEP/NCAR, NCEP-DOE AMIP-2, and JRA-25 reanalysis, Geophysical Research Letters, 33, 131–145, 2006.

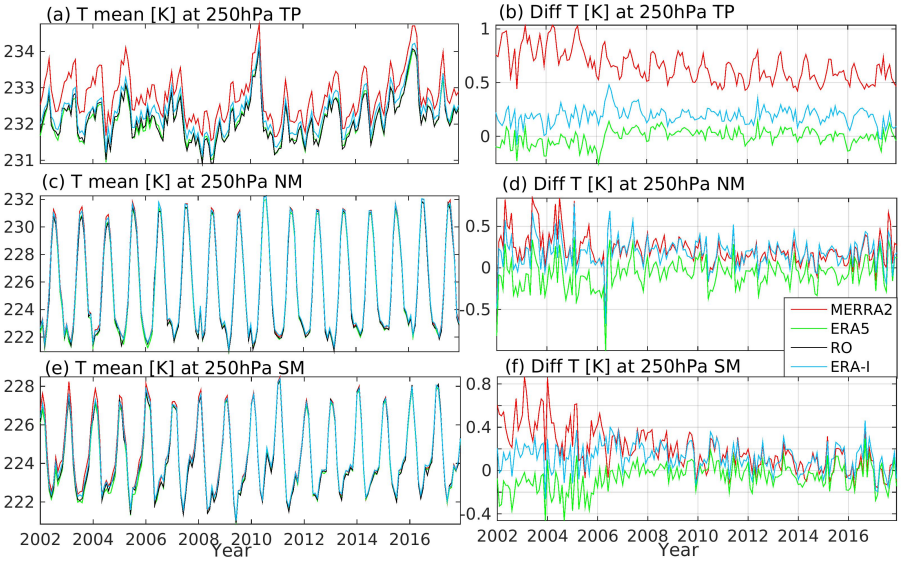

Figure 1. Left monthly mean temperature in K at pressure level 250 hPa through three latitude bands of tropics (TP) (10°S-10°N)(a), northern mid-latitudes (NM) (25°N-45°N) (c), southern mid-latitudes (SM) (25°S-45°S) (e); Right corresponding differences between three renanalyses and the GNSS RO in figures (b), (d) and (e); Model with 103 levels (margin), ERA5 (green), ERA-I (light blue), MERRA2 (red) and GNSS RO (black) are included.

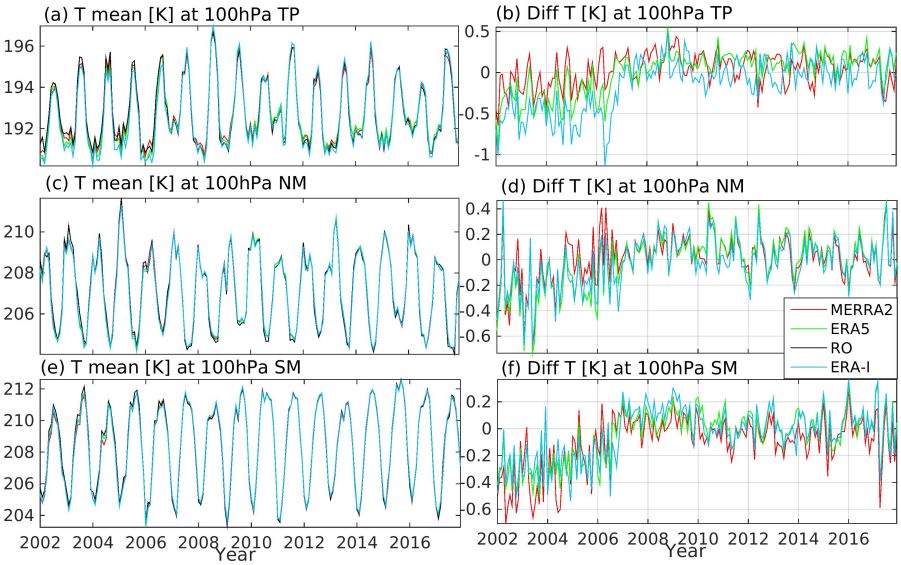

Figure 2. As in Figure 1 but for 100 hPa.

(

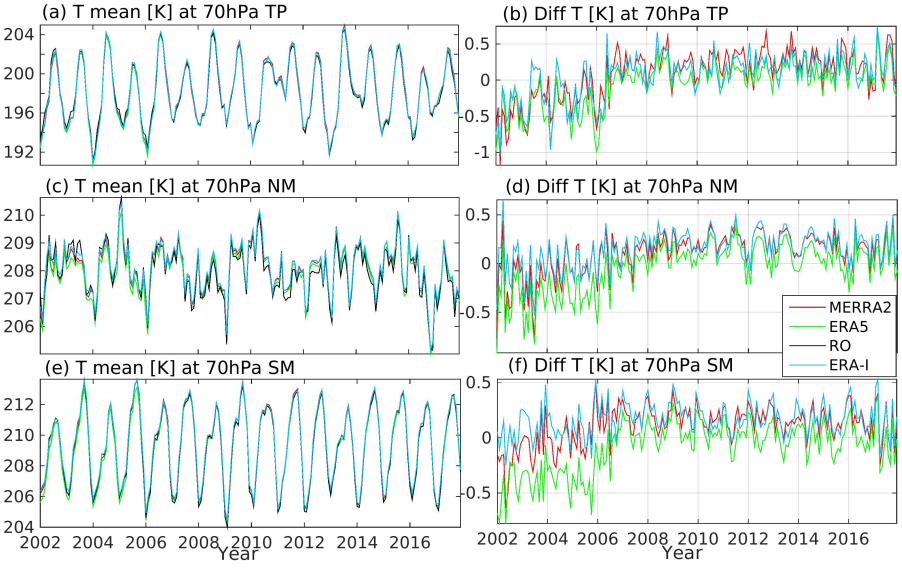

Figure 3. As in Figure 1 but for 70 hPa.

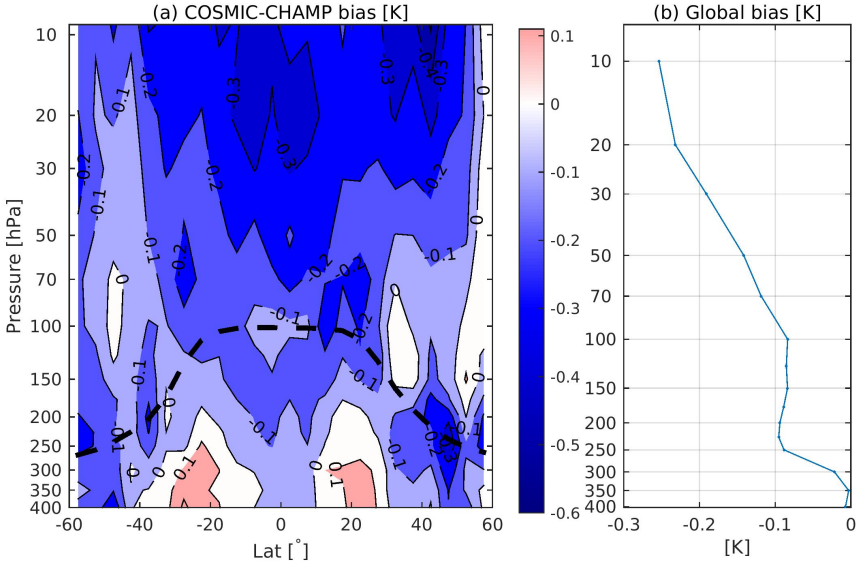

Figure 4. The bias in temperature climatology as retrieved from CHAMP and COSMIC RO data. The two missions obtained data during a 28 month overlap period from Jun. 2006 to Sep. 2008. (a) The difference of monthly zonal mean temperature; (b) The corresponding averaged difference for each layer. The dash black lines marked the tropopause height calcualted with GNSS RO data.

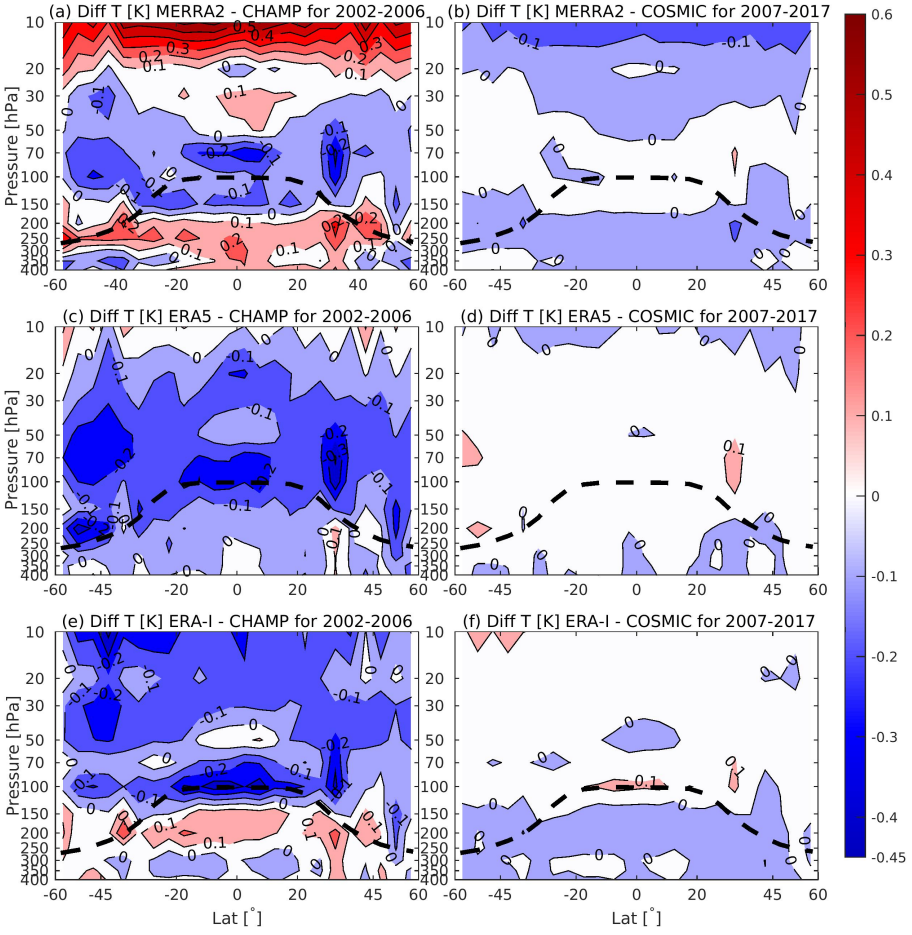

Figure 5. Differences of temperature anomalies between three reanalyses and CHAMP from 400 to 10 hPa for 2002-2006 (a, c and e) and between three renalayses and COSMIC for 2007-2017 (b, d and f). The dash black lines marked the tropopause height calcualted with GNSS RO data.

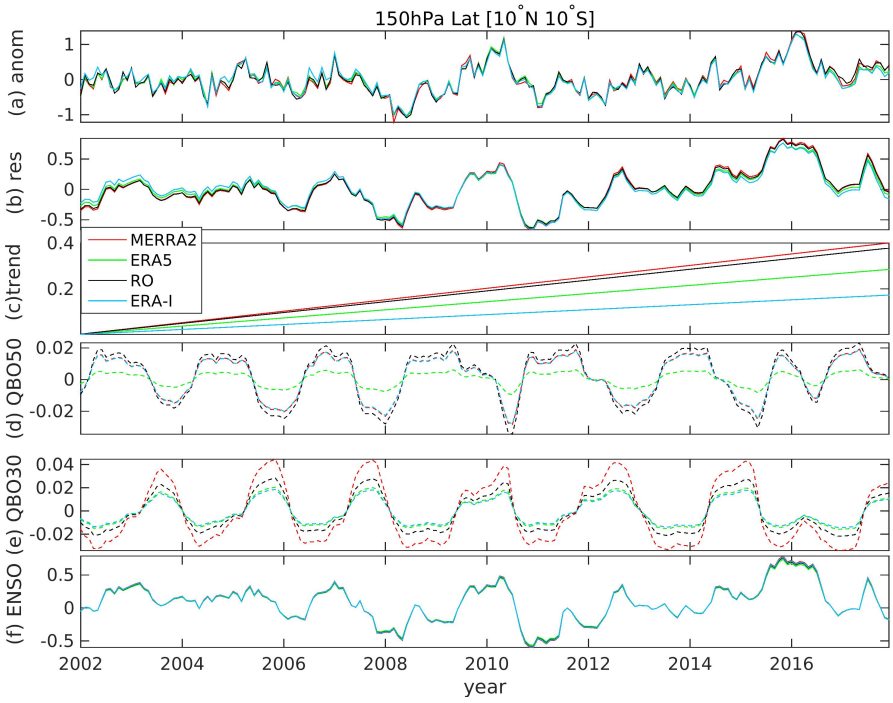

Figure 6. Temperature anomaly at pressure level 150 hPa in the tropics(10°S-10°N) from ERA5 (green), ERA-I (light blue), MERRA2 (red) and GNSS RO (black) (a); (b) The corresponding residual; (c) The linear terms; (d) The QBO50 terms; (e) The QBO30 terms and (f) the ENSO terms; The solid lines in (c-f) marked the siginificant terms and the dash lines in (c-f) marked the insiginifcant terms.

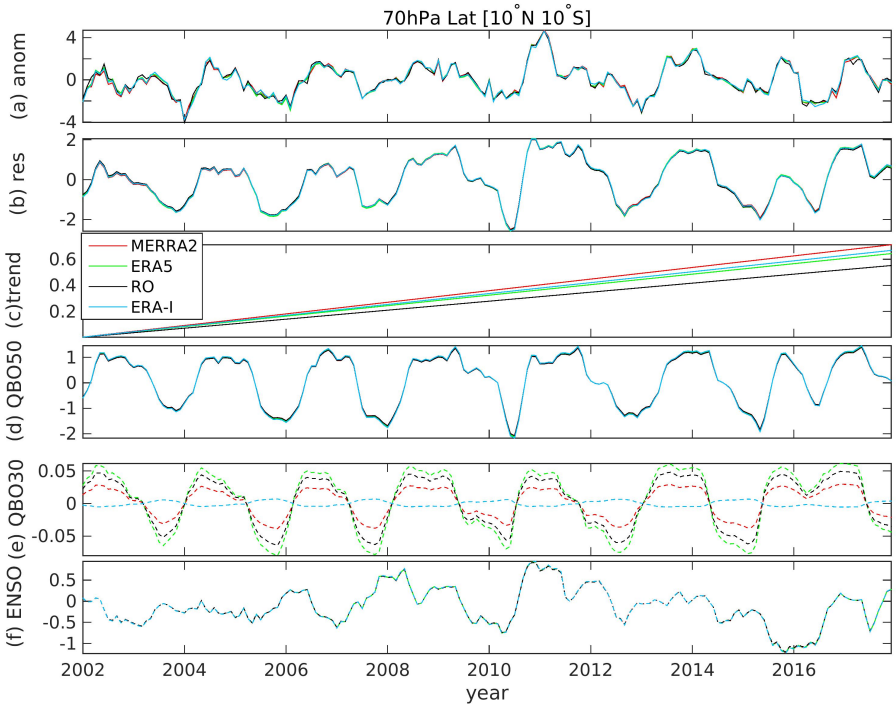

Figure 7. As in Figure 6 but for 70 hPa.

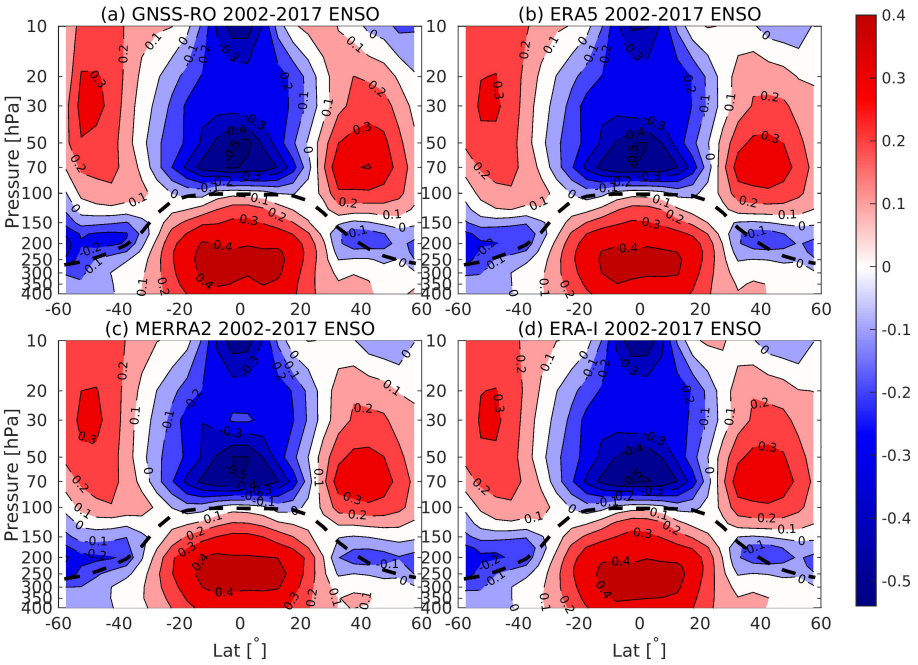

Figure 8. ENSO related temperature anomalies of GNSS RO (a), ERA5 (b), MERRA2 (c) and ERA-I (d). The dash black lines marked the tropopause height calcualted with GNSS RO data.

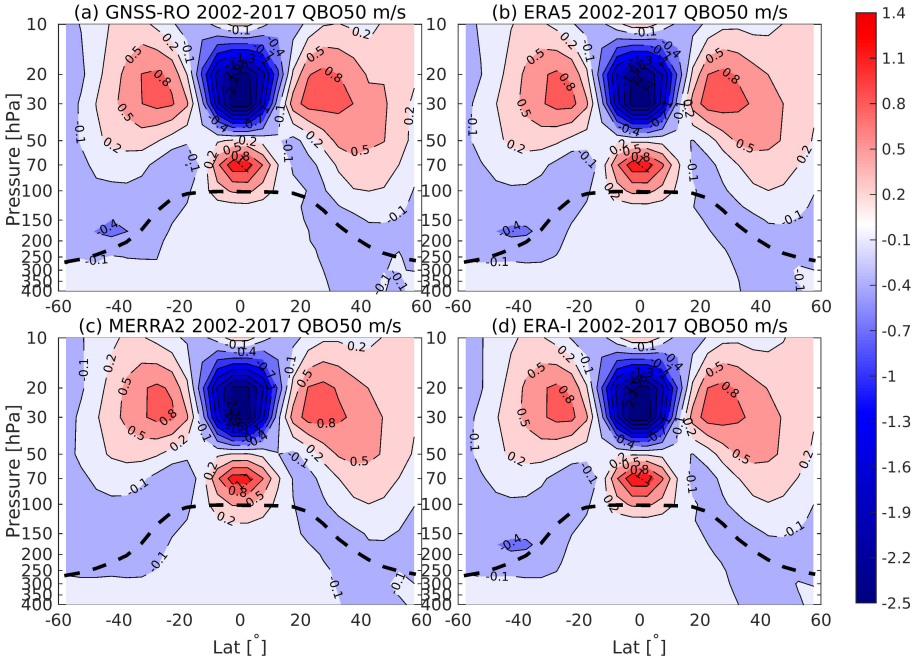

Figure 9. As in Figure 8 but for QBO50.

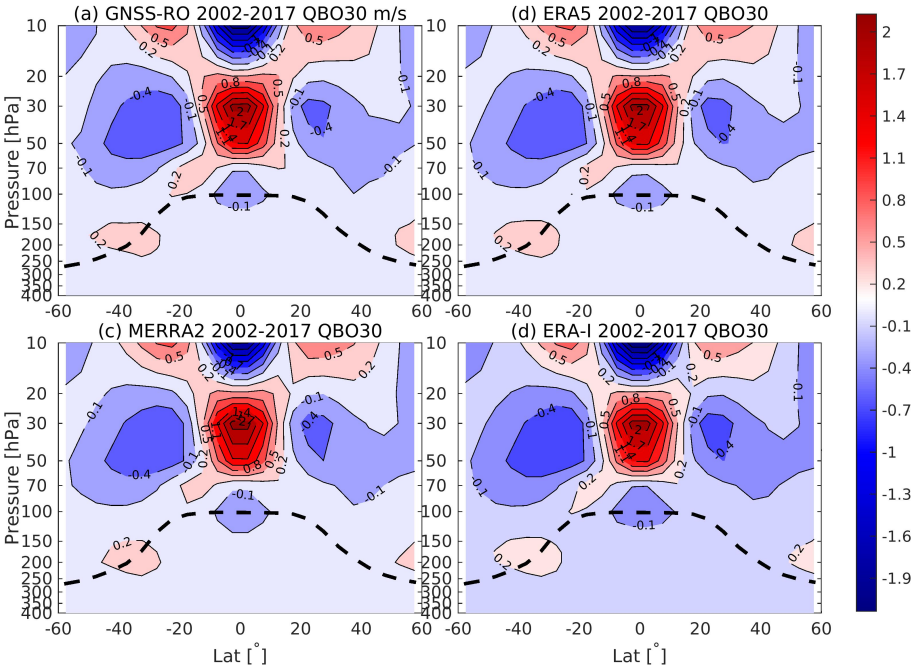

Figure 10. As in Figure 8 but for QBO30.

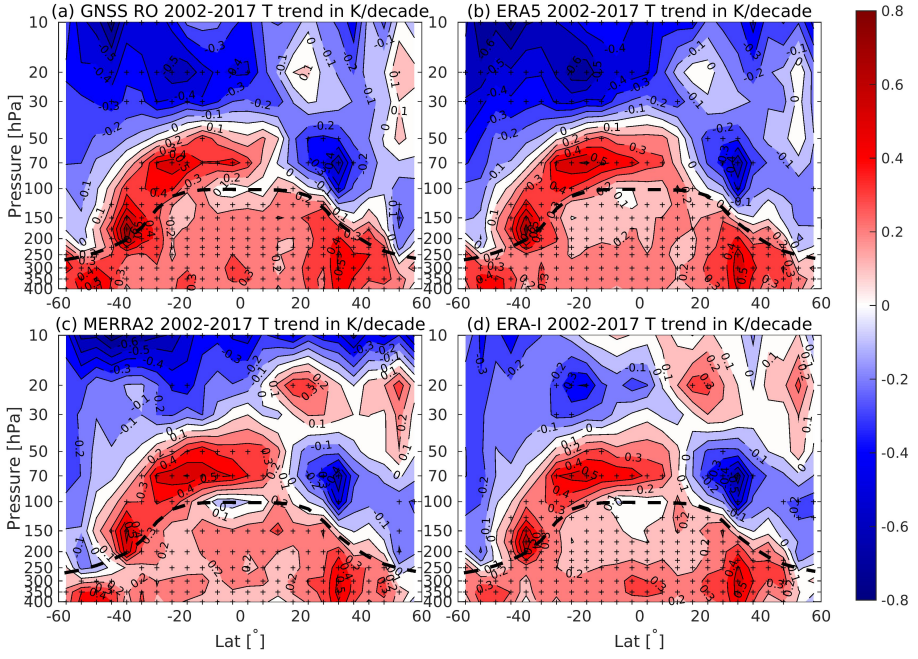

Figure 11. Temperature trend in K/decade based on GNSS RO (a), ERA5 (b), MERRA2 (c) and ERA-I (d) data for period 2002-2017. The '+' marked the significant area at 95% level. The dash black lines marked the tropopause height calcualted with GNSS RO data.

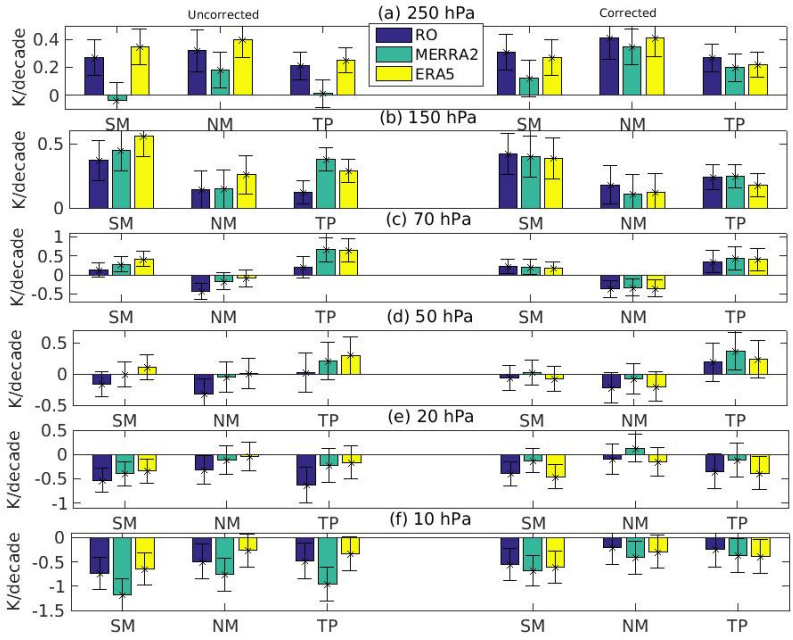

Figure 12. Estimated temperature trends in $\mathrm{K/decade}$ during different regions (SM: 25°S-45°S; NM: 25°N-45°N; TP: 10°S-10°N) from 2002 to 2017. (a-f) Trends in corrected and uncorrected data sets at 250, 150, 70, 50, 20 and 10hPa. Error bars represent 95% confidence intervals.

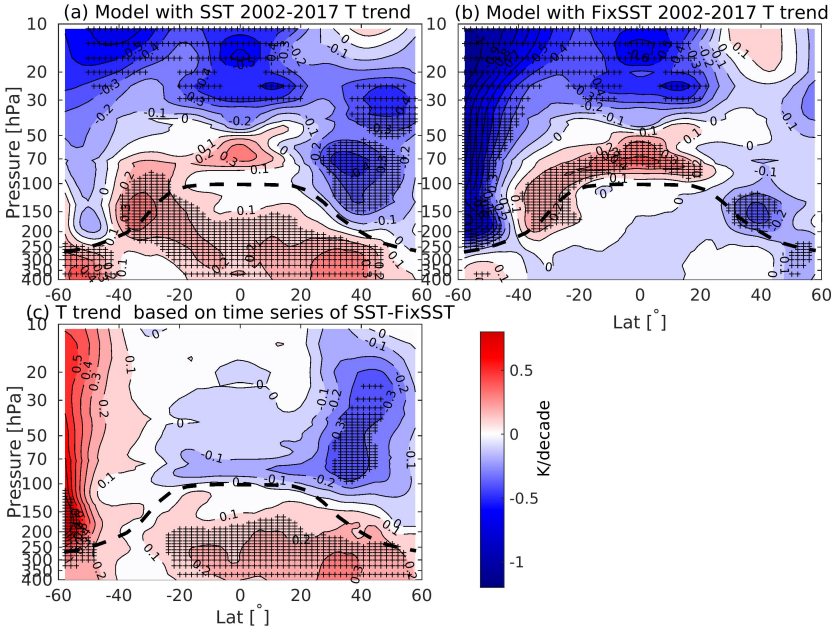

Figure 13. Temperature trend in $\mathrm{K}/\mathrm{decade}$ based on model simulations with time varying SST (a), fixSST (b) and their differences (c) for period 2002-2017. The '+' marked trends found to be more than 95% statistically significant. The dash black lines marked the tropopause height calcualted with GNSS RO data.

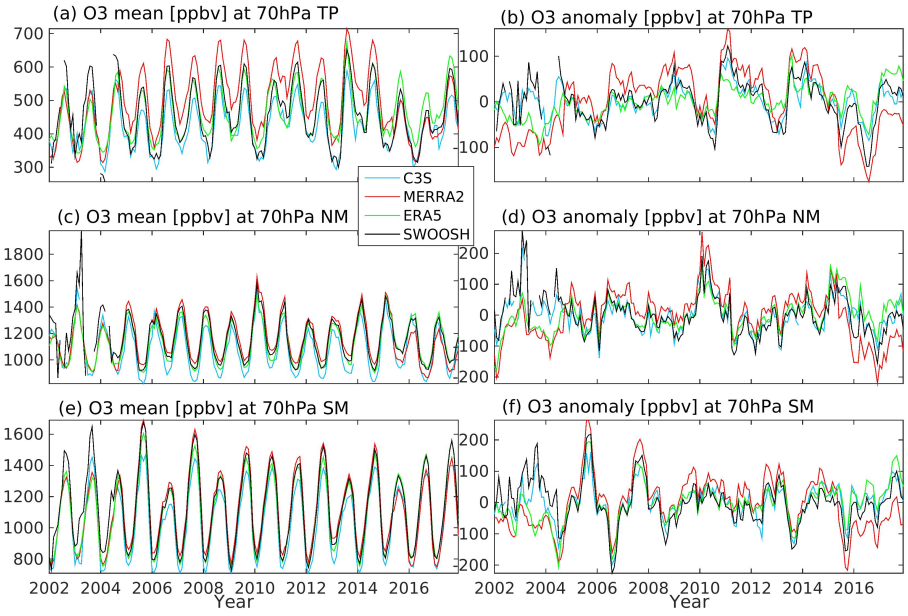

Figure 14. Left monthly mean ozone in ppbv at pressure level 70 hPa through three latitude bands of TP(10°S-10°N)(a), NM(25°N-45°N) (c), NM(25°S-45°S) (e); Right corresponding anomalies in figures (b), (d) and (e); Model with 103 levels (margin), ERA5 (green), C3S (light blue), MERRA2 (red) and SWOOSH (black) are included. The dash black lines marked the tropopause height calcualted with GNSS RO data.

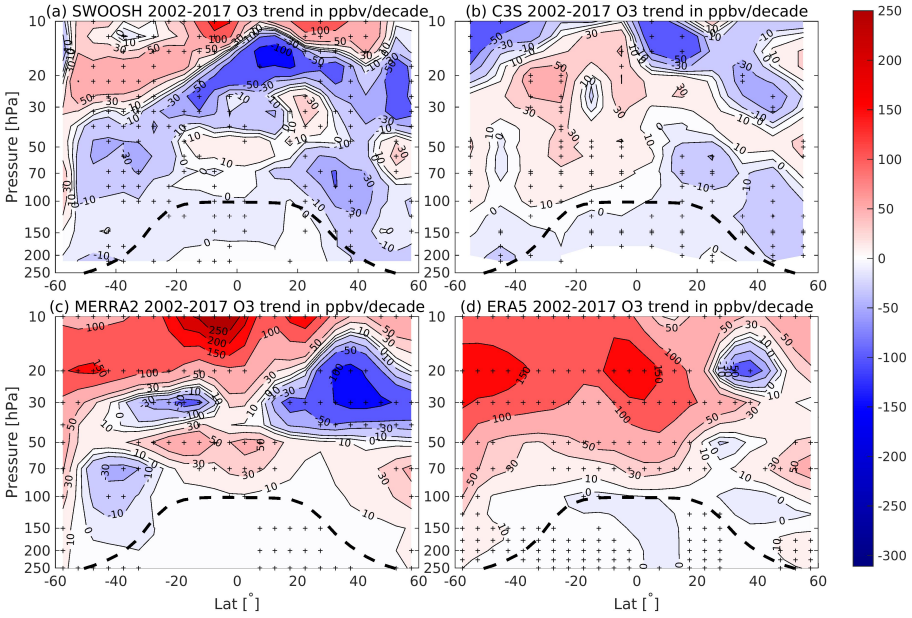

Figure 15. Ozone trend in ppbv/decade based on SWOOSH (a), ERA5 (b), MERRA2 (c) and C3S (d) data for period 2002-2017. The '+' marked trends found to be more than 95% statistically significant. The dash black lines marked the tropopause height calculated with GNSS RO data.

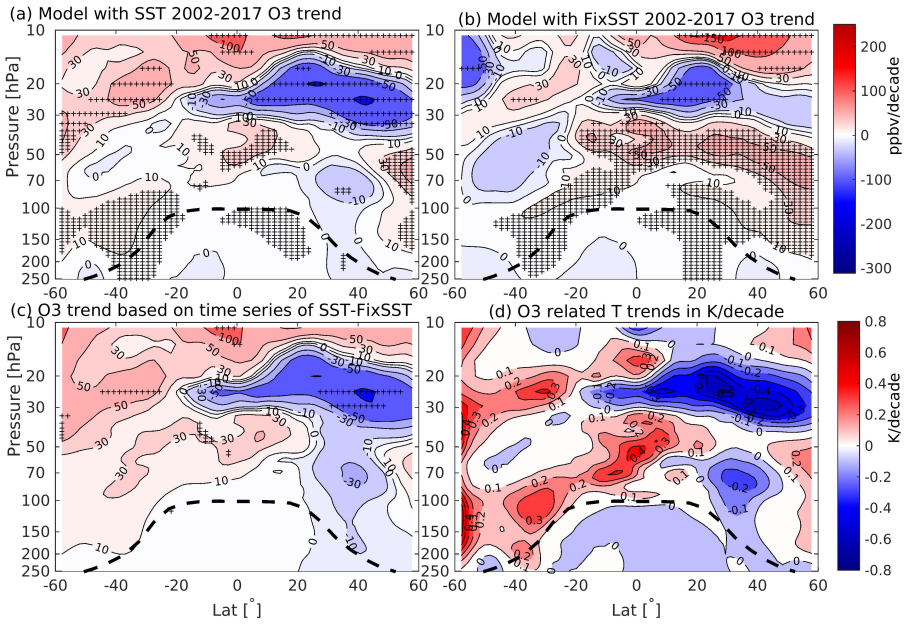

Figure 16. Ozone trend in ppbv/decade based on model simulations with time varying SST (a), FixSST (b) and thier differences SST-fixSST (c) for period 2002-2017. (d) Model ozone related GNSS RO temeprature trends in K/decade. The '+' marked trends found to be more than 95% statistically significant. The dash black lines marked the tropopause height calcualted with GNSS RO data.